International Journal of Mathematics and Computational Science
Vol. 4, No. 2, 2018, pp. 48-73
http://www.aiscience.org/journal/ijmcs
ISSN: 2381-7011 (Print); ISSN: 2381-702X (Online)

Numerical Elasticity Solution for Continuously Tapered and Arbitrarily Functionally Graded (FG) Rotating Disks via the Transfer Matrix Approach

Vebil Yıldırım*

Mechanical Engineering Department, University of Çukurova, Adana, Turkey

Abstract

The main purpose of the present study is to introduce the transfer matrix method, which is an efficacious and accurate analytical/numerical method developed based on the initial value problem (IVP), to numerically study the elastostatic response of variable-thickness rotating thin disks made of an isotropic but non-homogeneous material which is composed of a metal and a ceramic constituents under mechanical pressure and centrifugal forces. The governing equation called Navier equation of such disks having any arbitrary thickness profile is a second order non-homogeneous differential equation with variable coefficients. It is possible to achieve an analytical solution of Navier equation by using some certain material grading rules and certain disk profiles. Those certain conditions are out of the scope of the present study. The present study deals with the numerical solution of Navier equation developed for both arbitrarily functionally graded metal-ceramic pairs and arbitrarily continuously varying disk profiles. To this end, several conventional material grading rules such as a simple power rule (P-FGM), an exponential function (E-FGM), a linear function (L-FGM), a Voigt mixture rule with power of volume fractions of constituents (V-FGM), a Mori-Tanaka scheme (MT-FGM), and a sigmoid function (S-FGM) are all considered with several parabolically/linearly/hyperbolically tapered disk profiles including uniform ones. Three boundary conditions namely free-free, fixed-free, and fixed-fixed are examined. Some numerical results are also presented to serve benchmark solutions for future advanced studies for an aluminum/aluminum oxide (Al/Al_2O_3) FG material.

Keywords

Transfer Matrix Approach, Complementary Functions Method, Initial Value Problem,
Numerical Analysis, Axisymmetric Elasticity Solution, Rotating Variable-thickness Disk, Functionally Graded,
Inhomogeneous Material

Received: April 14, 2018 / Accepted: May 4, 2018 / Published online: June 6, 2018

1. Introduction

Rotating disks are commonly used as turbine rotors, compressors, flywheels, disk brakes, gears, computer disk drives, and etc. A good number of analytical/numerical studies on stationary/rotating discs with uniform/variable thickness and made of either traditional or advanced materials were reported in the available literature.

Guven [1], Eraslan [2-3], Apatay and Eraslan [4], Calderale et al. [5], Vivio et al. [6], Eraslan and Ciftci [7], and Argeso [8] were studied elastic analysis of variable thickness disks made of an isotropic and homogeneous materials.

Variable-thickness orthotropic disks were handled by Murthy and Sherbourne [9], Reddy and Srinath [10], Gurushankar [11], Zenkour and Allam [12], and Eraslan et al. [13].

Variable thickness orthotropic disks made of functionally

* Corresponding author
E-mail address: vebil@cu.edu.tr

graded materials (FGM) were examined by Kacar and Yıldırım [14], Essa and Argeso [15], Zheng et al. [16], and more recently by Yıldırım [17]. Under internal/external pressures and centrifugal forces, Yıldırım [17] developed unified formulas which are capable of exact determination of the elastic behavior of continuously hyperbolically tapered disks made of a single isotropic material, or made of a single polar orthotropic material, or made of a nonhomogeneous material formed by functionally power-law graded two isotropic materials, or a nonhomogeneous material formed by functionally power-law graded two orthotropic materials.

Elastic analysis of variable thickness disks made of functionally graded a metal and a ceramic phases also aroused attention to many investigators plus the author [18-33]. Eraslan and Akış [18] used a parabolic thickness variation for FGM solid disks. Vivio and Vullo [19] studied with rotating solid or annular conical disks. Vullo and Vivio [20] used a thickness variation with a power of linear function. By dividing the disc with varying thickness into sub-domains with uniform thickness, Bayat et al. [21] studied axisymmetric rotating hollow discs with parabolic and hyperbolic thickness profiles. Zenkour and Mashat [22] employed the modified Runge-Kutta algorithm to study the elastic analysis of variable thickness disks. Thermoelastic analysis of functionally graded rotating disks of variable thickness was considered by Tutuncu and Temel [23] based on the complementary functions method. Hassani et al. [24] worked on the thermomechanical analysis of rotating power-law graded hyperbolic disks under different boundary conditions by using semi-exact methods of Liao's homotopy analysis method. Based on a semi-analytical method, Bayat et al. [25] showed that a rotating concave parabolic disk graded with an exponential or Mori-Tanaka's scheme can be more efficient than the one with uniform thickness. Bayat et al. [26] considered two hollow parabolic disks made of a two sigmoid functionally graded materials under free-free and fixed-free boundary conditions. As in References [25-26], Ghorbani [27] used a semi-analytical solution technique in which the main domain is divided into virtual sub-domains having uniform properties. Amin et al. [28] used the finite difference method to study the thermo-mechanical analysis of FG rotating parabolic (convex, linear, and concave profiles) disks by using Voigt mixture of powers of volume fractions of constituents. Yıldırım [29] presented analytical formulas for the exact elastic response of a power-law graded rotating disk having a continuously varying hyperbolic thickness profile under different boundary conditions and under internal and external pressures including rotation at a constant angular velocity. Stress field in functionally graded (FG) rotating fixed-free disks with non-uniform thickness and variable angular velocity was studied numerically based on the finite difference method by Zheng et al. [30]. They used a thickness profile in the form of a rational function of the radial coordinate. Zheng et al. [30] showed that a smaller stress field can be developed by having ceramic rich composites at the outer radius. They also revealed that the deceleration in the angular velocity results in shear stress development within the disks without affecting the radial and circumferential stresses. Zheng et al.'s work [30], furthermore, revealed that the shear stress can cause a shift in the location of the maximum Von Mises stress, where for small deceleration, maximum Von Mises stress is located somewhere between the inner and outer radii, while for large deceleration it is located at the inner radius. Gang [31] analytically studied the stress analysis of simple-power law graded rotating convergent hyperbolic stress-free discs with negative inhomogeneity indexes. Yıldırım [32] investigated the effects of inhomogeneity and thickness parameters on the elastic response of a pressurized hyperbolic annulus/disc made of functionally graded material. In another study, Yıldırım [33] conducted a comprehensive parametric work for FGM hyperbolic disks subjected to the centrifugal forces at a constant rotational speed.

As seen from the literature survey that in the stress analysis of such disks, some certain material grading rules such as a simple power rule (P-FGM), an exponential function (E-FGM), a linear variation (L-FGM), Voigt mixture rule with power of volume fractions of constituents (V-FGM), Mori-Tanaka (MT-FGM), and a sigmoid function (S-FGM) have a preference. By employing above-mentioned favorable material grading rules, in the present study, the stress and displacement analyses of such disks having linearly, parabolically, and hyperbolically varying thickness profiles are to be conducted. The application of the transfer matrix method is to be also explained analytically for hollow disks made of isotropic and homogeneous materials and subjected to the mechanical pressure and centrifugal loads. Several formulas in closed forms, some of which overlaps Roark's [34] formulas have also been obtained as a result of this application under separate pressure and centrifugal forces acting on a hollow homogeneous uniform disk under four main boundary conditions. It is also aimed to study of the effects of thickness profiles on the elastic behavior of non-uniform disks made of a homogeneous and isotropic material to complete the context of the present study. Results are presented in both graphical and tabular forms.

2. Formulation and Solution of the Problem

In the present study the linear elastic analysis of such disks made of isotropic but nonhomogeneous material is to be

studied under axisymmetric plane stress and small deformations assumptions by using polar coordinates, (r,θ). In this case, the field equations are reduced to

$$\varepsilon_r(r)=\frac{du_r(r)}{dr} \tag{1}$$

$$\varepsilon_\theta(r)=\frac{u_r(r)}{r} \tag{2}$$

$$\sigma_r(r)=\frac{E(r)}{(1-\nu^2)}\varepsilon_r(r)+\frac{\nu E(r)}{(1-\nu^2)}\varepsilon_\theta(r) \tag{3}$$

$$\sigma_\theta(r)=\frac{\nu E(r)}{(1-\nu^2)}\varepsilon_r(r)+\frac{E(r)}{(1-\nu^2)}\varepsilon_\theta(r) \tag{4}$$

$$\frac{d}{dr}\big(rh(r)\sigma_r(r)\big)-h(r)\sigma_\theta(r)=-h(r)\rho(r)\omega^2 r \tag{5}$$

where $u_r(r)$ is the radial displacement, $\varepsilon_r(r)$ and $\varepsilon_\theta(r)$ are the radial and circumferential strains, $E(r)$ is Young's modulus, ν is Poisson's ratio, $\sigma_r(r)$ is the radial stress, $\sigma_\theta(r)$ is the hoop stress, ω is the angular velocity which is assumed to be unchanged, $\rho(r)$ is the material density, and $h(r)$ is the disk profile function. By making use of Eqs. (1)-(4), the equilibrium equation in Eq. (5) reads

$$\left(\begin{array}{l}\dfrac{d^2u_r(r)}{dr^2}\\ +\dfrac{du_r(r)}{dr}\left(\dfrac{1}{r}+\dfrac{\dfrac{dE(r)}{dr}}{E(r)}+\dfrac{\dfrac{dh(r)}{dr}}{h(r)}\right)\\ +u_r(r)\left(-\dfrac{1}{r^2}+\dfrac{\nu}{r}\left(\dfrac{\dfrac{dE(r)}{dr}}{E(r)}+\dfrac{\dfrac{dh(r)}{dr}}{h(r)}\right)\right)\end{array}\right)=-\frac{\rho(r)\omega^2 r(1-\nu^2)}{E(r)} \tag{6}$$

This is a second order differential equation called Navier equation with variable coefficients. It governs the elasto-static behavior of non-uniform disks made of any arbitrarily continuously graded isotropic material. In Eq. (6), the radial variation of Poisson's ratio is omitted.

Equation (6) is also a two-point boundary value problem (BVP). It is possible to get analytical solution to Navier equation under certain disk profiles and material grading rules. For arbitrary variations, the use of numerical solution techniques are involved. The state space, the complementary functions and the transfer matrix methods are bound up with the family of initial value problems (IVP).

A BVP problem governing with nth order differential equation may be solved by an IVP technique after putting the governing equation in the form of a set of n-ordinary differential equation with first order. When doing this, the state variables may be assigned in a few ways. The simplest and easiest choice is to use $u_r(r)$ and $du_r(r)/dr$ as principal state variables for Eq. (6). In the present study, choosing $u_r(r)$ and $\sigma_r(r)$ as principal state variables, Navier equation in Eq. (6) may be rewritten by two first order differential equation set as follows

$$\frac{du_r(r)}{dr}=-\frac{\nu}{r}u_r(r)+\frac{(1-\nu^2)}{E(r)}\sigma_r(r) \tag{7}$$

$$\frac{d\sigma_r(r)}{dr}=\frac{E(r)}{r^2}u_r(r)+\left(\frac{\nu-1}{r}-\frac{\dfrac{dh(r)}{dr}}{h(r)}\right)\sigma_r(r)-\rho(r)\omega^2 r \tag{8}$$

Equations (7) and (8) in a canonical form may be put in a matrix form as

$$\left\{\begin{array}{l}\dfrac{du_r(r)}{dr}\\ \dfrac{d\sigma_r(r)}{dr}\end{array}\right\}=\left[\begin{array}{ll}-\dfrac{\nu}{r} & \dfrac{1-\nu^2}{E(r)}\\ \dfrac{E(r)}{r^2} & \dfrac{\nu-1}{r}-\dfrac{\dfrac{dh(r)}{dr}}{h(r)}\end{array}\right]\left\{\begin{array}{l}u_r(r)\\ \sigma_r(r)\end{array}\right\}+\left\{\begin{array}{l}0\\ -\rho(r)\omega^2 r\end{array}\right\} \tag{9}$$

More compact form of Eq. (9) is

$$\frac{d}{dr}\mathrm{S}(r)=\mathrm{D}(r)\mathrm{S}(r)+\mathrm{k}(r)\ \ (0<a\le r\le b) \tag{10}$$

where $\mathrm{S}(r)$ is called the state vector containing the principal state variables, $\mathrm{D}(r)$ is the differential matrix. Column matrix $\mathrm{k}(r)$ represents the non-homogeneous terms in the differential equation.

By definition, the transfer matrix, $\mathrm{F}(a,r)$, is a matrix that attaches each state variable in the solution interval $0<a\le r\le b$ to the values of the state variables at the initial of the interval. In the absence of non-homogeneous terms, $\mathrm{k}(r)=0$, this relation is given by [35]

$$\mathrm{S}(r)=\mathrm{F}(a,r)\mathrm{S}(a)\ ,\quad a\le r\le b \tag{11}$$

From the definition, it is concluded that, at the beginning of the interval, the transfer matrix should take the values of the unit matrix, I.

$$\mathrm{F}(a,a)=\mathrm{I} \tag{12}$$

The transfer matrix satisfies the similar type of differential equation in Eq. (10) when $\mathrm{k}(r)$ =0 as follows

$$\frac{d}{dr}\mathrm{F}(a,r)=\mathrm{D}(r)\mathrm{F}(a,r) \tag{13}$$

The solution procedure strictly depends on the characteristics of the elements of the differential matrix. If those elements are constant, solution of the above equation under initial boundary conditions, $\mathrm{F}(a,a)=\mathrm{I}$, gives the transfer matrix as in the matrix exponential form

$$\mathrm{F}(a,r)=e^{r\mathrm{D}}=\mathrm{I}+r\mathrm{D}+\frac{r^2}{2!}\mathrm{D}^2+\frac{r^3}{3!}\mathrm{D}^3+\frac{r^4}{4!}\mathrm{D}^4+... \tag{14}$$

When the elements of D are not function of the radial coordinate anymore, then it is also possible to get the transfer matrix in a closed form by using several other methods. However if the elements of D are functions of the radial coordinate, then $\mathrm{F}(a,r)$ may be obtained numerically as in the present study. Similar to the finite elements, the numerical transfer matrix may be evaluated either in an approximate manner or in an accurate manner depending on the chosen numerical procedure. The author has previously achieved the accurate transfer matrices in numerical forms for some much more complex problems [36-37]. The same procedure having been employed by the author, therefore, is now to be originally applied for the static analysis of the variable-thickness FGM disks.

In the present study, the accurate numerical solution of Eq. (13) is found under boundary conditions in Eq. (12) with the help of the Complementary Functions Method (CFM) which is also one of the effective and accurate methods used for the initial value problem (IVP) solutions [38-42]. In the method of CFM, the general solution of BVP in Eq. (6) reads

$$u_r(r)=u_r^{(0)}(r)+b_1u_r^{(1)}(r)+b_2u_r^{(2)}(r) \tag{15}$$

Where $u_r^{(1)}(r)$ and $u_r^{(2)}(r)$ characterize the homogeneous solutions of Eq. (6) under prescribed kronecker delta initial conditions ($u_r(a)=1$ and $du_r(r)/dr|_{r=a}=0$ for the determination of $u_r^{(1)}(r)$; and $u_r(a)=0$ and $du_r(r)/dr|_{r=a}=1$ for the determination of $u_r^{(2)}(r)$) while $u_r^{(0)}(r)$ is the nonhomogeneous solutions of Eq. (6) under zero initial conditions ($u_r(a)=0$ and $du_r(r)/dr|_{r=a}=0$). In solution (15), b_1, and b_2 are the other unknowns which are determined by plugging the physical boundary conditions in the solution (15) [38-42].

After inserting Eqs. (1) and (2) into Eq. (3), the radial stress becomes

$$\sigma_r(r)=\frac{E(r)}{(1-\nu^2)}\frac{du_r(r)}{dr}+\frac{\nu E(r)}{(1-\nu^2)}\frac{u_r(r)}{r} \tag{16}$$

or by employing solution (15), it reads

$$\sigma_r(r)=\sigma_r^{(0)}(r)+b_1\sigma_r^{(1)}(r)+b_2\sigma_r^{(2)}(r) \tag{17}$$

CFM solutions in Eqs. (15) and (17) may be written in a compact form as

$$\begin{Bmatrix}u_r(r)\\ \sigma_r(r)\end{Bmatrix}=\begin{bmatrix}u_r^{(1)}(r) & u_r^{(2)}(r)\\ \sigma_r^{(1)}(r) & \sigma_r^{(2)}(r)\end{bmatrix}\begin{Bmatrix}b_1\\ b_2\end{Bmatrix}+\begin{Bmatrix}u_r^{(0)}(r)\\ \sigma_r^{(0)}(r)\end{Bmatrix} \tag{18}$$

To show that the CFM solutions inherently covers the fundamental matrix or the transfer matrix by alias, let's consider purely the homogeneous solution in Eq. (18) and write it for the inner surface.

$$\begin{Bmatrix}u_r(a)\\ \sigma_r(a)\end{Bmatrix}=\begin{bmatrix}u_r^{(1)}(a) & u_r^{(2)}(a)\\ \sigma_r^{(1)}(a) & \sigma_r^{(2)}(a)\end{bmatrix}\begin{Bmatrix}b_1\\ b_2\end{Bmatrix} \tag{19}$$

Now, let's isolate the unknown constants b_1 and b_2 from the above as

$$\begin{Bmatrix}b_1\\ b_2\end{Bmatrix}=\begin{bmatrix}u_r^{(1)}(a) & u_r^{(2)}(a)\\ \sigma_r^{(1)}(a) & \sigma_r^{(2)}(a)\end{bmatrix}^{-1}\begin{Bmatrix}u_r(a)\\ \sigma_r(a)\end{Bmatrix} \tag{20}$$

Substitution of Eq. (20) into (18) renders

$$\begin{Bmatrix}u_r(r)\\ \sigma_r(r)\end{Bmatrix}=\mathrm{F}(a,r)\begin{Bmatrix}u_r(a)\\ \sigma_r(a)\end{Bmatrix} \tag{21}$$

where $\mathrm{F}(a,r)$ is the transfer matrix or the fundamental matrix which is previously defined in Eq. (11). It's definition by CFM solutions turns to be

$$\mathrm{F}(a,r)=\begin{bmatrix}u_r^{(1)}(r) & u_r^{(2)}(r)\\ \sigma_r^{(1)}(r) & \sigma_r^{(2)}(r)\end{bmatrix}\begin{bmatrix}u_r^{(1)}(a) & u_r^{(2)}(a)\\ \sigma_r^{(1)}(a) & \sigma_r^{(2)}(a)\end{bmatrix}^{-1} \tag{22}$$

In the present study, in conclusion, the elements of the transfer matrix is obtained by the homogeneous solution of Eq. (9) under kronecker delta boundary conditions based on the complementary functions method [40-42]. As stated above, the accuracy of the numerical results are strictly depends on the accuracy of the numerical transfer matrix. In the present study, as it is to be seen in the following examples, the numerical results are achieved with a desired accuracy within the acceptable engineering errors.

Let's consider a uniform hollow disk made of an isotropic and homogeneous material. In this case, Eq. (6) takes the following form

$$\frac{d^2u_r(r)}{dr^2}+\frac{1}{r}\frac{du_r(r)}{dr}-\frac{1}{r^2}u_r(r)=0 \tag{23}$$

and the definition of the radial stress in Eq. (16) becomes

$$\sigma_r(r)=\frac{E}{(1-\nu^2)}\frac{du_r(r)}{dr}+\frac{\nu E}{(1-\nu^2)}\frac{u_r(r)}{r} \tag{24}$$

Analytical solution of Eq. (23) may be obtained as

$$u_r(r)=b_1r+\frac{b_2}{r} \tag{25}$$

From Eqs. (24) and (25) the following may be written

$$\begin{Bmatrix} u_r(r) \\ \sigma_r(r) \end{Bmatrix}=\begin{bmatrix} r & \frac{1}{r} \\ \frac{E}{1-\nu} & -\frac{E}{r^2(1+\nu)} \end{bmatrix}\begin{Bmatrix} b_1 \\ b_2 \end{Bmatrix}=\Phi(r)\begin{Bmatrix} b_1 \\ b_2 \end{Bmatrix} \tag{26}$$

Recalling Eq. (22)

$$\mathrm{F}(a,r)=\Phi(r)\Phi^{-1}(a) \tag{27}$$

and using the following

$$\Phi^{-1}(a)=\begin{bmatrix} \frac{1-\nu}{2a} & \frac{1-\nu^2}{2E} \\ \frac{a}{2}(1+\nu) & \frac{a^2}{2E}(\nu^2-1) \end{bmatrix} \tag{28}$$

the transfer matrix of a homogeneous hollow uniform disk may be derived in a closed form as follows [35].

$$\mathrm{F}(a,r)=\begin{bmatrix} \frac{a(1+\nu)}{2r}-\frac{r^2(\nu-1)}{2ar} & -\frac{(a^2-r^2)(1-\nu^2)}{2Er} \\ \frac{E}{2}(\frac{1}{a}-\frac{a}{r^2}) & \frac{\nu(r^2-a^2)+(a^2+r^2)}{2r^2} \end{bmatrix} \tag{29}$$

After derivation of the transfer matrix from the homogeneous solution of the governing equation, the complete solution of the problem is found by using the related procedure in the transfer matrix method. According to the procedure, the contribution of the nonhomogeneous term in Eq. (10), $\mathrm{k}(r)$, to Eq. (11) is expressed by adding the following integral $(a\le\xi\le b)$

$$\begin{aligned}\mathrm{S}(r)&=\mathrm{F}(a,r)\mathrm{S}(a)+\int_a^r \mathrm{F}(\xi,r)\mathrm{k}(\xi)d\xi \\ &=\mathrm{F}(a,r)\mathrm{S}(a)+\mathrm{K}(r)\end{aligned} \tag{30}$$

where, if the centrifugal forces are concerned

$$\mathrm{k}(\xi)=\begin{Bmatrix} 0 \\ -\rho\omega^2\xi \end{Bmatrix} \tag{31}$$

$$\mathrm{K}(r)=\int_a^r \mathrm{F}(\xi,r)\mathrm{k}(\xi)d\xi=\begin{Bmatrix} \int_a^r F_{1,2}(\xi,r)k_2(\xi)d\xi \\ \int_a^r F_{2,2}(\xi,r)k_2(\xi)d\xi \end{Bmatrix} \tag{32}$$

Recalling Eq. (29), Eq. (32) may be evaluated analytically for a homogeneous hollow uniform disk as follows

$$\begin{aligned}\mathrm{K}(r)&=\rho\omega^2\int_a^r\begin{Bmatrix} -\frac{(\xi^2-r^2)(1-\nu^2)}{2Er} \\ \frac{\nu(r^2-\xi^2)+(\xi^2+r^2)}{2r^2} \end{Bmatrix}\xi d\xi \\ &=\rho\omega^2\begin{Bmatrix} -\frac{(1-\nu^2)}{2Er}\int_a^r(\xi^2-r^2)\xi d\xi \\ \frac{\nu}{2r^2}\int_a^r(r^2-\xi^2)\xi d\xi+\frac{1}{2r^2}\int_a^r(r^2+\xi^2)\xi d\xi \end{Bmatrix} \\ &=\begin{Bmatrix} \frac{\rho\omega^2(a^2-r^2)^2(\nu^2-1)}{8Er} \\ -\frac{\rho\omega^2(a^2-r^2)(a^2(\nu-1)-r^2(\nu+3))}{8r^2} \end{Bmatrix}\end{aligned} \tag{33}$$

In the present study, the gauss quadrature numerical integration technique is used to evaluate Eq. (32) [36].

Equation (30) states that when both the elements of the initial state vector and the transfer matrix are all known, elastic fields at any surface of the disks may be computed. It is known that, the elements of both $\mathrm{F}(a,r)$ and $\mathrm{k}(r)$ are already known. In this case, the unknown elements of $\mathrm{S}(a)$ is determined by considering the physical boundary conditions given at both the inner and outer surfaces. To do this, Eq. (30) is written for $r=b$ as follows

$$\begin{aligned}u_r(b)&=F_{1,1}(a,b)u_r(a)+F_{1,2}(a,b)\sigma_r(a) \\ &\quad+\int_a^b F_{1,2}(\xi,b)k_2(\xi)d\xi\end{aligned} \tag{34}$$

$$\begin{aligned}\sigma_r(b)&=F_{2,1}(a,b)u_r(a)+F_{2,2}(a,b)\sigma_r(a) \\ &\quad+\int_a^b F_{2,2}(\xi,b)k_2(\xi)d\xi\end{aligned} \tag{35}$$

From the above equations, the unknown element of the state vector at the initial surface may be found. To find the unknown initial radial displacement, an appropriate one of the followings

$$u_r(a) = \frac{u_r(b) - F_{1,2}(a,b)\sigma_r(a) - \int_a^b F_{1,2}(\xi,b)k_2(\xi)d\xi}{F_{1,1}(a,b)} \quad (36)$$

$$u_r(a) = \frac{\sigma_r(b) - F_{2,2}(a,b)\sigma_r(a) - \int_a^b F_{2,2}(\xi,b)k_2(\xi)d\xi}{F_{2,1}(a,b)} \quad (37)$$

or to find the initial radial stress, an appropriate one of the followings

$$\sigma_r(a) = \frac{u_r(b) - F_{1,1}(a,b)u_r(a) - \int_a^b F_{1,2}(\xi,b)k_2(\xi)d\xi}{F_{1,2}(a,b)} \quad (38)$$

$$\sigma_r(a) = \frac{\sigma_r(b) - F_{2,1}(a,b)u_r(a) - \int_a^b F_{2,2}(\xi,b)k_2(\xi)d\xi}{F_{2,2}(a,b)} \quad (39)$$

is used. For instance, for a homogeneous hollow uniform disk, if one consider just the internal and external pressure loads ($\omega = 0$) (Figure 1), the initial state vector is found by substituting the corresponding boundary conditions, $\sigma_r(a) = -p_a$ and $\sigma_r(b) = -p_b$, into Eq. (37) as follows

$$\mathrm{S}(a) = \begin{Bmatrix} u_r(a) \\ \sigma_r(a) \end{Bmatrix} = \begin{Bmatrix} \dfrac{-p_b + F_{2,2}(a,b)p_a - \int_a^b F_{2,2}(\xi,b)k_2(\xi)d\xi}{F_{2,1}(a,b)} \\ -p_a \end{Bmatrix} = \begin{Bmatrix} \dfrac{-p_b + p_a\left(\left(\frac{\nu+1}{2b^2}\right)b^2 - \frac{a^2(\nu-1)}{2b^2}\right)}{\frac{E}{2}\left(\frac{1}{a} - \frac{a}{b^2}\right)} \\ -p_a \end{Bmatrix} \quad (40)$$

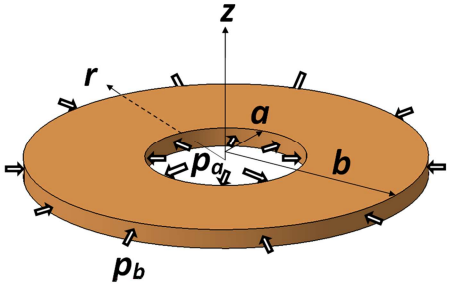

Figure 1. A uniform disk subjected to the internal and external pressures.

Plugging Eq. (40) into Eq. (30) gives the following formulas which overlaps with Roark's formulas in the open literature [34].

$$\begin{aligned} u_r(r) &= -p_a \frac{a^2\left(\nu(b^2 - r^2) + (b^2 + r^2)\right)}{Er(a^2 - b^2)} \\ &\quad + p_b \frac{b^2\left(\nu(a^2 - r^2) + (a^2 + r^2)\right)}{Er(a^2 - b^2)} \\ &= -p_a \frac{a^2\left(b^2(\nu+1) - (\nu-1)r^2\right)}{Er(a^2 - b^2)} \\ &\quad + p_b \frac{b^2\left(a^2(\nu+1) - (\nu-1)r^2\right)}{Er(a^2 - b^2)} \end{aligned} \quad (41)$$

$$\sigma_r(r) = p_a \frac{a^2(b^2 - r^2)}{r^2(a^2 - b^2)} - p_b \frac{b^2(a^2 - r^2)}{r^2(a^2 - b^2)} \quad (42)$$

$$\begin{aligned} \sigma_\theta(r) &= \frac{E}{1-\nu^2}\left(\nu\frac{du_r(r)}{dr} + \frac{u_r(r)}{r}\right) \\ &= -p_a \frac{a^2(b^2 + r^2)}{r^2(a^2 - b^2)} + p_b \frac{b^2(a^2 + r^2)}{r^2(a^2 - b^2)} \end{aligned} \quad (43)$$

where

$$\begin{aligned} \frac{du_r(r)}{dr} &= p_a \frac{a^2\left(\nu(b^2 + r^2) + (b^2 - r^2)\right)}{Er^2(a^2 - b^2)} \\ &\quad - p_b \frac{b^2\left(\nu(a^2 + r^2) + (a^2 - r^2)\right)}{Er^2(a^2 - b^2)} \end{aligned} \quad (44)$$

For a homogeneous uniform stress-free disk (FF) rotating at a constant angular velocity ($\omega \neq 0$, $p_a = p_b = 0$) (Figure 2), under boundary conditions $\sigma_r(a) = 0$ and $\sigma_r(b) = 0$, the whole elements of the initial state vector is obtained by using Eq. (37) as

$$\mathrm{S}^{(FF)}(a) = \begin{Bmatrix} u_r(a) \\ \sigma_r(a) \end{Bmatrix} = \begin{Bmatrix} \dfrac{-\int_a^b F_{2,2}(\xi,b)k_2(\xi)d\xi}{F_{2,1}(a,b)} \\ 0 \end{Bmatrix} = \begin{Bmatrix} \dfrac{-\rho\omega^2\frac{(a^2 - b^2)}{8b^2}\left(b^2(\nu+3) + a^2(1-\nu)\right)}{\frac{E}{2}\left(\frac{1}{a} - \frac{a}{b^2}\right)} \\ 0 \end{Bmatrix} \quad (45)$$

and then the followings formulas may be developed to consider just the effect of centrifugal forces on elastic fields in a FF-disk.

$$u_r^{(FF)}(r)=\frac{\rho\omega^2}{8Er}\begin{pmatrix}a^2(\nu+3)\left(b^2(\nu+1)-(\nu-1)r^2\right)\\-(\nu-1)r^2\left(b^2(\nu+3)-(\nu+1)r^2\right)\end{pmatrix} \quad (46)$$

$$\sigma_r^{(FF)}(r)=\frac{(3+\nu)}{8r^2}\rho\omega^2(a^2-r^2)(r^2-b^2) \quad (47)$$

$$\sigma_\theta^{(FF)}(r)=\frac{\rho\omega^2}{8r^2}\begin{pmatrix}a^2(3+\nu)(b^2+r^2)\\+r^2\left(b^2(\nu+3)-(1+3\nu)r^2\right)\end{pmatrix} \quad (48)$$

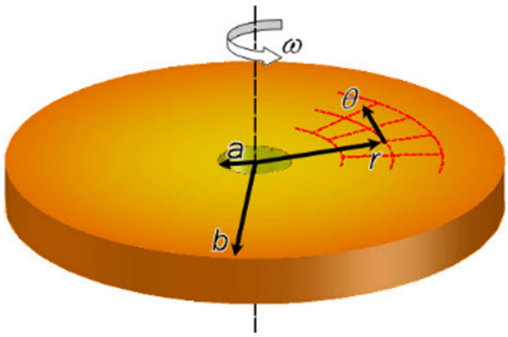

Figure 2. A uniform rotating stress-free (FF) disk.

It may be easily verified that Eqs. (46-48) overlap the corresponding Roark's formulas [34].

$$u_{r-ROARK}(r)=\frac{(3+\nu)}{8}\rho\omega^2 r\frac{(1-\nu)}{E}\begin{pmatrix}a^2+b^2-\dfrac{(1+\nu)}{(3+\nu)}r^2\\+\dfrac{(1+\nu)}{(1-\nu)}\dfrac{a^2b^2}{r^2}\end{pmatrix} \quad (49)$$

$$\sigma_{r-ROARK}(r)=\frac{(3+\nu)}{8}\rho\omega^2\left(b^2+a^2-\frac{a^2b^2}{r^2}-r^2\right) \quad (50)$$

$$\sigma_{\theta-ROARK}(r)=\frac{(3+\nu)}{8}\rho\omega^2\left(b^2+a^2-\frac{(1+3\nu)}{(3+\nu)}r^2+\frac{a^2b^2}{r^2}\right) \quad (51)$$

It is worth noting that, Eq. (37) may also be written for combined pressure and centrifugal loads.

For a homogeneous uniform rotating CF-disk mounted on a rotating rigid shaft at its center ($\omega\neq 0,\ p_a=p_b=0$) (Figure 3), the clamped-free boundary conditions, $u_r(a)=0$ and $\sigma_r(b)=0$, are to be used in Eq. (39)

$$S^{(CF)}(a)=\begin{Bmatrix}u_r(a)\\\sigma_r(a)\end{Bmatrix}=\begin{Bmatrix}0\\-\dfrac{\int_a^b F_{2,2}(\xi,b)k_2(\xi)d\xi}{F_{2,2}(a,b)}\end{Bmatrix} \quad (52)$$
$$=\begin{Bmatrix}0\\-\rho\omega^2\dfrac{(a^2-b^2)((\nu+3)b^2-a^2(\nu-1))}{4((\nu+1)b^2-a^2(\nu-1))}\end{Bmatrix}$$

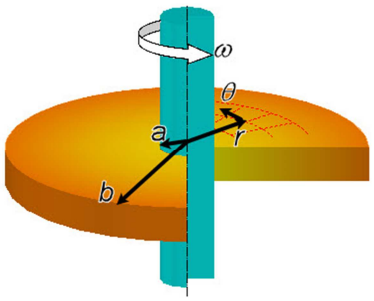

Figure 3. A uniform rotating mounted disk (CF).

The variations of the elastic fields along the radial coordinate are expressed by

$$u_r^{(CF)}(r)=\frac{\rho\omega^2(a^2-r^2)(1-\nu^2)}{8Er\left((\nu+1)b^2-a^2(\nu-1)\right)}\begin{pmatrix}a^2\left(b^2(\nu+1)-(\nu-1)r^2\right)\\+b^2\left(r^2(\nu+1)-(\nu+3)b^2\right)\end{pmatrix} \quad (53)$$

$$\sigma_r^{(CF)}(r)=\frac{\rho\omega^2(r^2-b^2)}{8r^2\left((\nu-1)a^2-b^2(\nu+1)\right)}\begin{pmatrix}a^4(\nu^2-1)\\-a^2(\nu-1)(\nu+3)\\(b^2+r^2)\\+b^2(\nu+1)r^2(\nu+3)\end{pmatrix} \quad (54)$$

$$\sigma_\theta^{(CF)}(r)=\frac{\rho\omega^2}{8r^2\left((\nu-1)a^2-b^2(\nu+1)\right)}\begin{pmatrix}a^4(\nu^2-1)(b^2+r^2)\\-a^2(\nu-1)\\\left(b^4(\nu+3)+(3\nu+1)r^4\right)\\-b^2(\nu+1)r^2\\\left(b^2(\nu+3)-(3\nu+1)r^2\right)\end{pmatrix} \quad (55)$$

For a homogeneous uniform rotating CC-disk mounted on a rotating rigid shaft at its center and having a rigid casing at the outer surface ($\omega\neq 0,\ p_a=p_b=0$) (Figure 4), the clamped-clamped boundary conditions, $u_r(a)=0$ and $u_r(b)=0$, are to be used in Eq. (38)

$$S^{(CC)}(a)=\begin{Bmatrix}u_r(a)\\\sigma_r(a)\end{Bmatrix}=\begin{Bmatrix}0\\-\dfrac{\int_a^b F_{1,2}(\xi,b)k_2(\xi)d\xi}{F_{1,2}(a,b)}\end{Bmatrix} \quad (56)$$
$$=\begin{Bmatrix}0\\-\rho\omega^2\dfrac{(a^2-b^2)}{4}\end{Bmatrix}$$

The variations of the elastic fields along the radial coordinate may be derived in a closed form as follows

$$u_r^{(CC)}(r)=\frac{\rho\omega^2}{8Er}(a^2-r^2)(b^2-r^2)(\nu^2-1) \quad (57)$$

$$\sigma_r^{(CC)}(r)=\frac{\rho\omega^2}{8r^2}\begin{pmatrix}-(\nu+3)r^4+(1-\nu)a^2b^2\\+(\nu+1)a^2r^2+(\nu+1)b^2r^2\end{pmatrix} \quad (58)$$

$$\sigma_{\theta}^{(CC)}(r)=\frac{\rho\omega^2}{8r^2}\begin{pmatrix}-(3\nu+1)r^4-(1-\nu)a^2b^2\\+(\nu+1)a^2r^2+(\nu+1)b^2r^2\end{pmatrix} \quad (59)$$

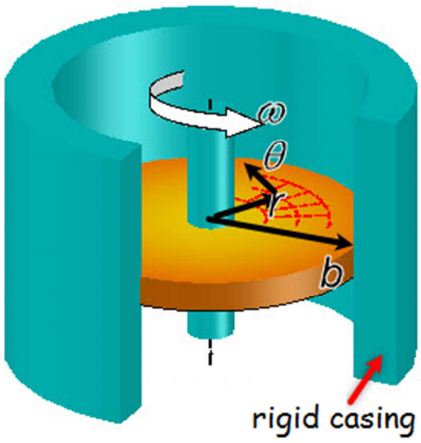

Figure 4. A uniform rotating mounted disk having a rigid casing at the outer surface (CC).

3. Disk Geometrical and Material Properties

In the present study, four different frequently used and more generalized disk thickness profile functions picked up from the literature are to be examined. Let $a>0$ is the inner radius, and $b>a>0$ is the outer radius of the disk. In the present study, unless otherwise stated, $a=0.2m$ and $b=1.0m$ are to be used in numerical computations.

A hyperbolic disk profile which is also called Stodola's disk is given by

$$h(r)=h_o(\frac{r}{b})^m \quad (60)$$

In Eq. (60) $m>0$ suggests divergent hyperbolic profiles, $m<0$ offers convergent disk profiles, $m=1$ is a linearly varying divergent disk profile, and $m=0$ overlaps the uniform disk profile.

A two-parameter parabolic profile function reads

$$h(r)=h_o\left(1-n\left(\frac{r}{b}\right)^m\right) \quad (61)$$

where $0\le n<1$ and $m>0$. One may obtain a uniform profile with $n=0$, a convex profile with $m>1$, a concave profile with $0<m<1$, and a linear profile with $m=1$.

As a final disk profile, a conical thickness variation is employed.

$$h(r)=h_o\left(1-\frac{r}{nb}\right) \quad (62)$$

The disk profile variations with Eqs. (60)-(62) are presented in Figure 5. To obtain a concrete idea from the results of those disk geometries, all profile parameters have been arranged in such a way that their maximum thicknesses will be the same.

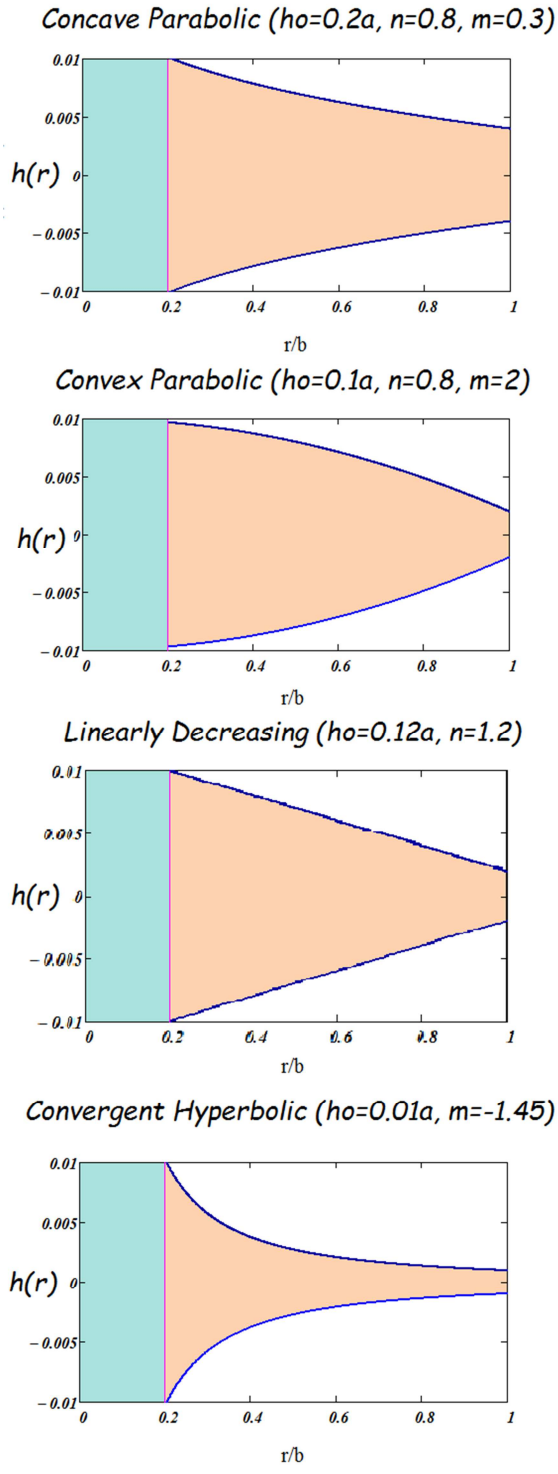

Figure 5. Thickness profiles considered in the present study.

Now, let's introduce commonly used material grading rules. In the present study an Aluminum (Al) metal and an Aluminum Oxide (Al_2O_3) ceramic are functionally graded along the radial coordinate. It is supposed that the metal is to be full at the inner surface and the ceramic is to be full at the outer surface by observing Zheng's et al.'s suggestion [30]. The individual mechanical properties of those materials are:

$$E_m = E_{Al} = 70\ GPa\ ,\ E_c = E_{Al_2O_3} = 393.0\ GPa$$

$$\rho_{Al} = 2700\ kg/m^3\ ,\ \rho_c = \rho_{Al_2O_3} = 3970\ kg/m^3$$

$$\nu_m = \nu_{Al} = 0.3\ ,\ \nu_c = \nu_{Al_2O_3} = 0.3$$

A simple power grading rule (P-FGM) may be defined by

$$E(r)_{P-FGM} = E_m(\frac{r}{a})^{\frac{\ln(E_m/E_c)}{\ln(a/b)}} \tag{63}$$

$$\rho(r)_{P-FGM} = \rho_m(\frac{r}{a})^{\frac{\ln(\rho_m/\rho_c)}{\ln(a/b)}} \tag{64}$$

The following form of an exponential grading rule (E-FGM) is to be observed in the present study.

$$E(r)_{E-FGM} = E_m e^{\frac{(r-a)}{(a-b)}\ln(E_m/E_c)} \tag{65}$$

$$\rho(r)_{E-FGM} = \rho_m e^{\frac{(r-a)}{(a-b)}\ln(E_m/E_c)} \tag{66}$$

For linear variations of the effective properties (L-FGM) are in the form of

$$E(r)_{L-FGM} = E_c\left(1-\left(1-\frac{E_m}{E_c}\right)\left(\frac{r-b}{a-b}\right)\right) \tag{67}$$

$$\rho(r)_{L-FGM} = \rho_c\left(1-\left(1-\frac{\rho_m}{\rho_c}\right)\left(\frac{r-b}{a-b}\right)\right) \tag{68}$$

Based on the simple Voigt mixture rule, the radial variation of the effective material properties (V-FGM) are defined by an inhomogeneity parameter, $n \geq 0$.

$$E(r)_{V-FGM} = (E_c - E_m)\left(\frac{r-a}{b-a}\right)^n + E_m \tag{69}$$

$$\rho(r)_{V-FGM} = (\rho_c - \rho_m)\left(\frac{r-a}{b-a}\right)^n + \rho_m \tag{70}$$

In the above equations, $n = 1$ corresponds a linear variation. $n < 1$ presents a mixture which is much richer in ceramic towards the outer surface.

Mori-Tanaka rule may be used to estimate the effective mechanical properties of a graded microstructure which has a ceramic and a metal phase. In Mori-Tanaka estimate (MT-FGM), the equivalent elasticity modulus of FGM can be given in terms of the effective bulk modulus $K(r)$ and the effective shear modulus $G(r)$ of FG material as follows [25]

$$\rho(r)_{MT-FGM} = (\rho_c - \rho_m)\left(\frac{r-a}{b-a}\right)^n + \rho_m \ \ ;\ \ n \geq 0 \tag{71}$$

$$E(r)_{MT-FGM} = \frac{9K(r)G(r)}{3K(r)+G(r)} \tag{72}$$

where

$$G(r) = \frac{\left(\frac{r-a}{b-a}\right)^n (G_c - G_m)}{1+\left(1-\left(\frac{r-a}{b-a}\right)^n\right)\frac{(G_c-G_m)}{G_m + \frac{(9K_m+8G_m)G_m}{6(K_m+2G_m)}}} + G_m \tag{73}$$

$$K(r) = \frac{\left(\frac{r-a}{b-a}\right)^n (K_c - K_m)}{1+\left(1-\left(\frac{r-a}{b-a}\right)^n\right)\frac{(K_c-K_m)}{K_m + \frac{4}{3}G_m}} + K_m \tag{74}$$

and bulk and shear moduli of the ceramic and metal constituents are

$$K_m = \frac{E_m}{3(1-2\nu_m)}\ ,\ K_c = \frac{E_c}{3(1-2\nu_c)} \tag{75}$$

$$G_m = \frac{E_m}{2(1+\nu_m)}\ ,\ G_c = \frac{E_c}{2(1+\nu_c)} \tag{76}$$

A sigmoid function originally proposed by Chung and Chi [43] is composed of two power-law functions to define a new volume fractions as follows

$$V_c^I(r) = 1 - \frac{\left(-\frac{2b-2r}{a-b}\right)^p}{2}\ ,\ (\frac{a+b}{2} \leq r \leq b) \tag{77}$$

$$V_c^{II}(r) = \frac{\left(\frac{2a-2r}{a-b}\right)^p}{2}\ ,\ (a \leq r \leq \frac{a+b}{2}) \tag{78}$$

where the superscripts I defines the region of $(a+b)/2 \leq r \leq b$, and II determines the region of $a \leq r \leq (a+b)/2$. By using Eqs. (77) and (78) the variations of Young's modulus and the material density may be written as

$$E^{I}_{S-FGM}(r) = V^{I}_{c}(r)E_c + \left(1 - V^{I}_{c}(r)\right)E_m \quad (79)$$

$$E^{II}_{S-FGM}(r) = V^{II}_{c}(r)E_c + \left(1 - V^{II}_{c}(r)\right)E_m \quad (80)$$

and

$$\rho^{I}_{S-FGM}(r) = V^{I}_{c}(r)\rho_c + \left(1 - V^{I}_{c}(r)\right)\rho_m \quad (81)$$

$$\rho^{II}_{S-FGM}(r) = V^{II}_{c}(r)\rho_c + \left(1 - V^{II}_{c}(r)\right)\rho_m \quad (82)$$

In Eqs. (77)-(82), $p = 1$ proposes a linear variation. S-FGM was originally used in Bayat et al.'s study for parabolic disks [26]. This rule is to be used for hyperbolic thickness profiles as the first time in the literature.

4. Validation of the Results

In this section, the present results are to be validated by analytical solutions of a convergent hyperbolic disk made of either a homogeneous material or a power-law graded material (P-FGM) under centrifugal forces. The necessary data and corresponding dimensionless elastic fields for three boundary conditions are comparatively presented in Tables 1-3. From Tables 1-3, it is observed that the results are in perfect harmony with each other.

Table 1. Comparison of the present numerical results of a rotating FF-disk with the analytical ones in the open literature.

$\frac{r}{b}$	Yıldırım [33] (Analytical)	Present	Yıldırım [33] (Analytical)	Present
	Convergent Hyperbolic / Isotropic and homogeneous material $h(r) = h_o(r/a)^{-1}$		Convergent Hyperbolic P-FGM $h(r) = h_o(r/a)^{-1}$, $E(r) = E_a(r/a)^{-5}$, $\rho(r) = \rho_a(r/a)^{-5}$	
$\overline{u_r}(r) = E_a u_r(r)/(\rho_a \omega^2 b^3)$				
0.2	0.0940756	0.094075	0.0156245	0.015618
0.4	0.0974064	0.097406	0.0159332	0.015918
0.6	0.122101	0.122101	0.0245572	0.024411
0.8	0.143166	0.143166	0.0387422	0.038011
1.0	0.146899	0.146899	0.0469333	0.046930
$\overline{\sigma_r}(r) = \sigma_r(r)/(\rho_a \omega^2 b^2)$				
0.2	0.	0.000000	0.	0.000000
0.4	0.192345	0.192344	0.0012097	0.001204
0.6	0.207334	0.207332	0.0003335	0.000326
0.8	0.138135	0.138134	0.0000924	0.000086
1.0	0.	0.000000	0.	0.000000
$\overline{\sigma_\theta}(r) = \sigma_\theta(r)/(\rho_a \omega^2 b^2)$				
0.2	0.470378	0.470376	0.0781227	0.078091
0.4	0.301219	0.301218	0.0016077	0.001605
0.6	0.265702	0.265701	0.0002685	0.000265
0.8	0.220399	0.220397	0.0000750	0.000072
1.0	0.146899	0.146899	0.0000150	0.000015

5. Results and Discussion

In this section, a great many problems are to be solved with the help of the transfer matrix approach. Dimensionless results having been obtained by Eqs. (80)-(82) are to be represented by both graphical and tabular forms.

Table 2. Comparison of the present numerical results of a rotating CF-disk with the analytical ones in the open literature.

$\frac{r}{b}$	Yıldırım [33] (Analytical)	Present	Yıldırım [33] (Analytical)	Present
	Convergent Hyperbolic / Isotropic and homogeneous material $h(r) = h_o(r/a)^{-1}$		Convergent Hyperbolic P-FGM $h(r) = h_o(r/a)^{-1}$, $E(r) = E_a(r/a)^{-5}$, $\rho(r) = \rho_a(r/a)^{-5}$	
$\overline{u_r}(r) = E_a u_r(r)/(\rho_a \omega^2 b^3)$				
0.2	0.	0.000000	0.	0.000000
0.4	0.0402527	0.040253	0.0043763	0.004370
0.6	0.0782458	0.078246	0.014864	0.014783
0.8	0.105641	0.105641	0.0301576	0.029715

$\frac{r}{b}$	Yıldırım [33] (Analytical)	Present	Yıldırım [33] (Analytical)	Present
	Convergent Hyperbolic / Isotropic and homogeneous material $h(r)=h_o(r/a)^{-1}$		Convergent Hyperbolic P-FGM $h(r)=h_o(r/a)^{-1}$, $E(r)=E_a(r/a)^{-5}$, $\rho(r)=\rho_a(r/a)^{-5}$	
1.0	0.1125	0.112500	0.039021	0.039021
$\overline{\sigma_r}(r)=\sigma_r(r)/(\rho_a\omega^2b^2)$				
0.2	0.224944	0.224944	0.0115991	0.011597
0.4	0.253716	0.253716	0.0013435	0.001340
0.6	0.231579	0.231580	0.0003430	0.000339
0.8	0.146828	0.146828	0.0000936	0.000090
1.0	0.	0.000000	0.	0.000000
$\overline{\sigma_\theta}(r)=\sigma_\theta(r)/(\rho_a\omega^2b^2)$				
0.2	0.0674831	0.067483	0.0034797	0.003479
0.4	0.176747	0.176747	0.0007450	0.000743
0.6	0.199884	0.199884	0.0002049	0.000203
0.8	0.1761	0.176100	0.0000649	0.000063
1.0	0.1125	0.112500	0.0000125	0.000012

Table 3. Comparison of the present numerical results of a rotating CC-disk with the analytical ones in the open literature.

$\frac{r}{b}$	Yıldırım [33] (Analytical)	Present	Yıldırım [33] (Analytical)	Present
	Convergent Hyperbolic / Isotropic and homogeneous material $h(r)=h_o(r/a)^{-1}$		Convergent Hyperbolic P-FGM $h(r)=h_o(r/a)^{-1}$, $E(r)=E_a(r/a)^{-5}$, $\rho(r)=\rho_a(r/a)^{-5}$	
$\overline{u_r}(r)=E_a u_r(r)/(\rho_a\omega^2b^3)$				
0.2	0.	0.000000	0.	0.000000
0.4	0.0212162	0.021216	0.00427	0.004264
0.6	0.0343044	0.034304	0.013407	0.013326
0.8	0.0304735	0.030474	0.020876	0.020433
1.0	0.	0.000000	0.	0.000000
$\overline{\sigma_r}(r)=\sigma_r(r)/(\rho_a\omega^2b^2)$				
0.2	0.130418	0.130418	0.0115523	0.011550
0.4	0.118566	0.118566	0.0012815	0.001278
0.6	0.053102	0.053102	0.0002690	0.000265
0.8	-0.072735	-0.072735	0.0000098	0.000006
1.0	-0.258515	-0.258515	-0.000092	-0.000092
$\overline{\sigma_\theta}(r)=\sigma_\theta(r)/(\rho_a\omega^2b^2)$				
0.2	0.0391253	0.039125	0.0034657	0.003465
0.4	0.0886103	0.088610	0.0007180	0.000717
0.6	--	0.073105	--	0.000171
0.8	--	0.016272	--	0.000027
1.0	--	-0.077555	--	-0.000028

$$\overline{\sigma_r}(r)=\frac{1}{\rho_c\omega^2b^2+p_a}\sigma_r(r) \tag{83}$$

$$\overline{\sigma_\theta}(r)=\frac{1}{\rho_c\omega^2b^2+p_a}\sigma_\theta(r) \tag{84}$$

$$\overline{u_r}(r)=\frac{E_c}{\rho_c\omega^2b^3+bp_a}u_r(r) \tag{85}$$

In Eqs. (83)-(85), p_a represents the internal pressure. In the present study, four types of thickness profiles plus uniform one are considered with six material grading rules. Profile parameters in the disk profiles considered in the present study (Figure 5) are given in Table 4.

Table 4. Disk profiles (Figure 5) and corresponding profile parameters.

No		h_o	n	m
1	Hyperbolic	0.01a	--	-1.45
2	Parabolic-I	0.2a	0.8	0.3
3	Parabolic-II	0.1a	0.8	2
4	Linear	0.12a	1.2	--

The variation of the effective elasticity modulus along the

radial coordinate with the material grading rules is illustrated in Figure 6. For an aluminum/aluminum oxide FGM material, this figure suggests that there is no significant difference in the variation of Young's modulus between L-FGM and P-FGM since the inhomogeneity parameter of the P-FGM rule takes a value much closer to the unit, $\ln(E_m/E_c)/\ln(a/b)=1.072$. However, there will be a difference in the variation of the material density between L-FGM and P-FGM since $\ln(\rho_m/\rho_c)/\ln(a/b)=0.24$.

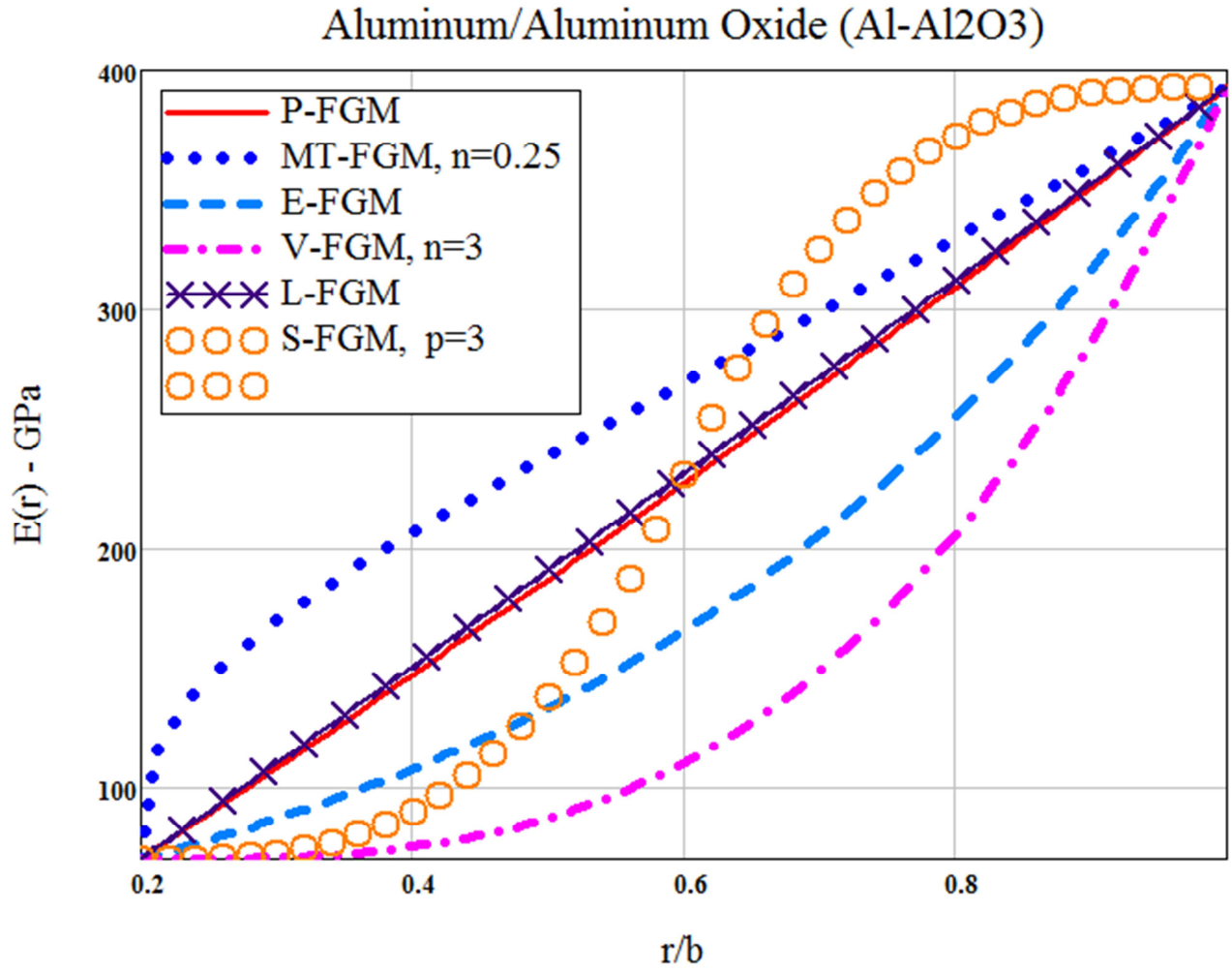

Figure 6. Radial variation of the effective Young's modulus.

Table 5. Comparison of the thickness profiles of a FF-disk made of an isotropic and homogeneous material under centrifugal forces.

r/b	HYP	PAR-I	PAR-II	LINEAR	UNI
			$\bar{u}_r$		
0.2	0.072605	0.122218	0.116096	0.107387	0.166400
0.4	0.076223	0.123393	0.115688	0.107601	0.166465
0.6	0.099625	0.146141	0.132984	0.125806	0.191360
0.8	0.121179	0.164486	0.146337	0.140850	0.208812
1.	0.126311	0.166409	0.147423	0.142977	0.208000
			$\bar{\sigma}_r$		
0.2	0.000000	0.000000	0.000000	0.000000	0.000000
0.4	0.164787	0.208016	0.178241	0.173477	0.259874
0.6	0.192701	0.205889	0.166097	0.170131	0.234666
0.8	0.135761	0.133437	0.107451	0.114430	0.139218
1.	0.000000	0.000000	0.000000	0.000000	0.000000
			$\bar{\sigma}_\theta$		

r/b	HYP	PAR-I	PAR-II	LINEAR	UNI
0.2	0.363024	0.611091	0.580477	0.536933	0.831998
0.4	0.239994	0.370888	0.342693	0.321045	0.494124
0.6	0.223852	0.305336	0.271470	0.260715	0.389332
0.8	0.192201	0.245638	0.215157	0.210391	0.302781
1.	0.126311	0.166409	0.147423	0.142977	0.208000
			$\bar{\sigma}_{eq}$		
0.2	0.363024	0.611091	0.580477	0.536933	0.831998
0.4	0.212612	0.321990	0.296861	0.278335	0.428115
0.6	0.210017	0.269731	0.237052	0.229262	0.339536
0.8	0.171111	0.212994	0.186332	0.182438	0.262498
1.	0.126311	0.166409	0.147423	0.142977	0.208000

As a first examination, effects of the thickness profiles of FF/CF/CC disks made of an isotropic and homogeneous material under separate internal pressure and centrifugal forces are investigated. Results are demonstrated in Tables 5-8 and Figures 7-10.

Table 6. Comparison of the thickness profiles of a FF-disk made of an isotropic and homogeneous material under pressure loads.

r/b	HYP	PAR-I	PAR-II	LINEAR	UNI
			$\bar{u}_r$		
0.2	0.491288	0.327326	0.303925	0.325339	0.276666
0.4	0.310788	0.186966	0.171302	0.187703	0.147082
0.6	0.242218	0.141551	0.131131	0.144441	0.107777
0.8	0.208265	0.120912	0.113277	0.124683	0.091041
1.	0.191034	0.110844	0.104190	0.114586	0.083333
			$\bar{\sigma}_r$		
0.2	-1.00000	-1.00000	-1.00000	-1.000000	-1.000000
0.4	-0.29229	-0.22839	-0.20447	-0.212229	-0.218752
0.6	-0.12215	-0.08220	-0.06630	-0.072303	-0.074076
0.8	-0.04609	-0.02808	-0.02149	-0.024649	-0.023439
1.	0.000000	0.000000	0.000000	0.000000	0.000000
			$\bar{\sigma}_\theta$		
0.2	2.156440	1.336628	1.219626	1.326693	1.083328
0.4	0.689281	0.398898	0.366915	0.405589	0.302080
0.6	0.367053	0.211321	0.198661	0.219045	0.157405
0.8	0.246506	0.142717	0.135151	0.148459	0.106769
1.	0.191034	0.110844	0.104190	0.114586	0.083333
			$\bar{\sigma}_{eq}$		
0.2	2.794042	2.030567	1.925387	2.021586	1.804696
0.4	0.872935	0.549897	0.501454	0.543711	0.452974
0.6	0.441000	0.262119	0.238819	0.262766	0.204752
0.8	0.272487	0.158631	0.147075	0.162194	0.120215
1.	0.191034	0.110844	0.104190	0.114586	0.083333

Table 7. Comparison of the thickness profiles of a mounted disk (CF) made of an isotropic and homogeneous material under centrifugal forces.

r/b	HYP	PAR-I	PAR-II	LINEAR	UNIFORM
			$\bar{u}_r$		
0.2	0.000000	0.000000	0.000000	0.000000	0.000000
0.4	0.030293	0.053583	0.050253	0.045644	0.078002
0.6	0.063829	0.093288	0.082894	0.078129	0.126538
0.8	0.090400	0.119339	0.103067	0.099695	0.154056
1.	0.098079	0.125021	0.107624	0.105155	0.157880

r/b	HYP	PAR-I	PAR-II	LINEAR	UNIFORM
			$\bar{\sigma}_r$		
0.2	0.147785	0.373384	0.381987	0.330076	0.601447
0.4	0.207983	0.293294	0.256345	0.243529	0.391442
0.6	0.210752	0.236504	0.191424	0.193996	0.279219
0.8	0.142572	0.143921	0.115658	0.122566	0.153316
1.	0.000000	0.000000	0.000000	0.000000	0.000000
			$\bar{\sigma}_\theta$		
0.2	0.044335	0.112015	0.114596	0.099023	0.180434
0.4	0.138129	0.221946	0.202536	0.187170	0.312439
0.6	0.169608	0.226432	0.195584	0.188414	0.294662
0.8	0.155772	0.192350	0.163531	0.161389	0.238565
1.	0.098079	0.125021	0.107624	0.105155	0.157880
			$\bar{\sigma}_{eq}$		
0.2	0.131354	0.331871	0.339518	0.293378	0.534577
0.4	0.183325	0.264926	0.234125	0.220811	0.358529
0.6	0.193489	0.231632	0.193538	0.191266	0.287252
0.8	0.149609	0.173287	0.145621	0.145904	0.209387
1.	0.098079	0.125021	0.107624	0.105155	0.157880

Table 8. Comparison of the thickness profiles of a CC-disk made of an isotropic and homogeneous material under centrifugal forces.

	MOUNTED AND WITH RIGID CASING DISK (CC)				
r/b	HYP	PAR-I	PAR-II	LINEAR	UNI
			$\bar{u}_r$		
0.2	0.000000	0.000000	0.000000	0.000000	0.000000
0.4	0.018177	0.025630	0.028969	0.026497	0.028665
0.6	0.031884	0.037632	0.042205	0.039599	0.038827
0.8	0.029950	0.032015	0.038315	0.035927	0.030713
1.	0.000000	0.000000	0.000000	0.000000	0.000000
			$\bar{\sigma}_r$		
0.2	0.097887	0.193438	0.232753	0.203736	0.240000
0.4	0.111629	0.124105	0.134789	0.128316	0.124875
0.6	0.060935	0.044824	0.055250	0.055190	0.030222
0.8	-0.063700	-0.08071	-0.07062	-0.07087	-0.08953
1.	-0.264754	-0.26908	-0.42139	-0.35871	-0.24000
			$\bar{\sigma}_\theta$		
0.2	0.029366	0.058031	0.069826	0.061121	0.072000
0.4	0.078930	0.101307	0.112859	0.104737	0.109125
0.6	0.071420	0.076167	0.086917	0.082554	0.073778
0.8	0.018328	0.015806	0.026708	0.023649	0.011531
1.	-0.079426	-0.08072	-0.12642	-0.10761	-0.07200
			$\bar{\sigma}_{eq}$		
0.2	0.087004	0.171931	0.206875	0.181085	0.213317
0.4	0.099399	0.114422	0.125272	0.118302	0.117793
0.6	0.066797	0.066306	0.076190	0.072835	0.064240
0.8	0.074573	0.089665	0.087100	0.085191	0.095819
1.	0.235319	0.239165	0.374541	0.318830	0.213317

Von-Mises equivalent stress at any surface of the disk is obtained by

$$\sigma_{eq} = \sqrt{\sigma_r^2 - \sigma_r \sigma_\theta + \sigma_\theta^2} \tag{86}$$

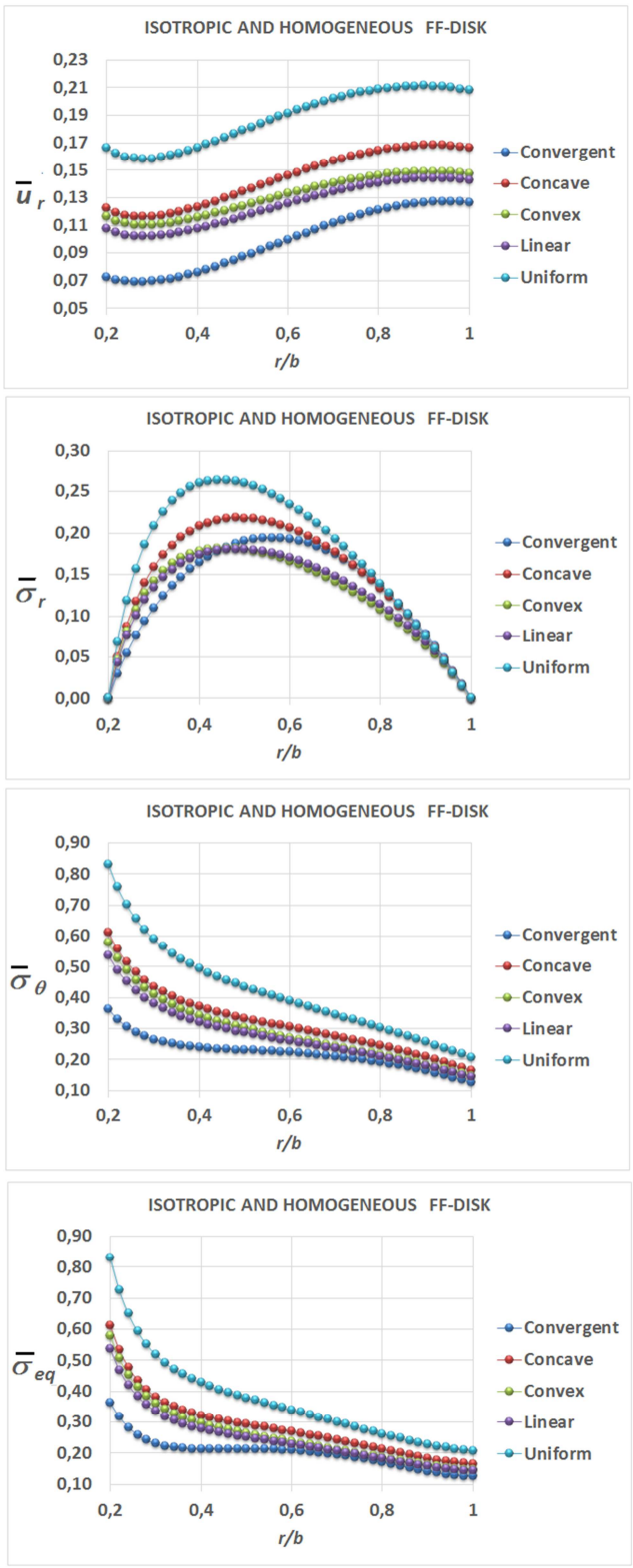

Figure 7. Elastic fields in a non-uniform FF-disk made of an isotropic and homogeneous material under centrifugal forces.

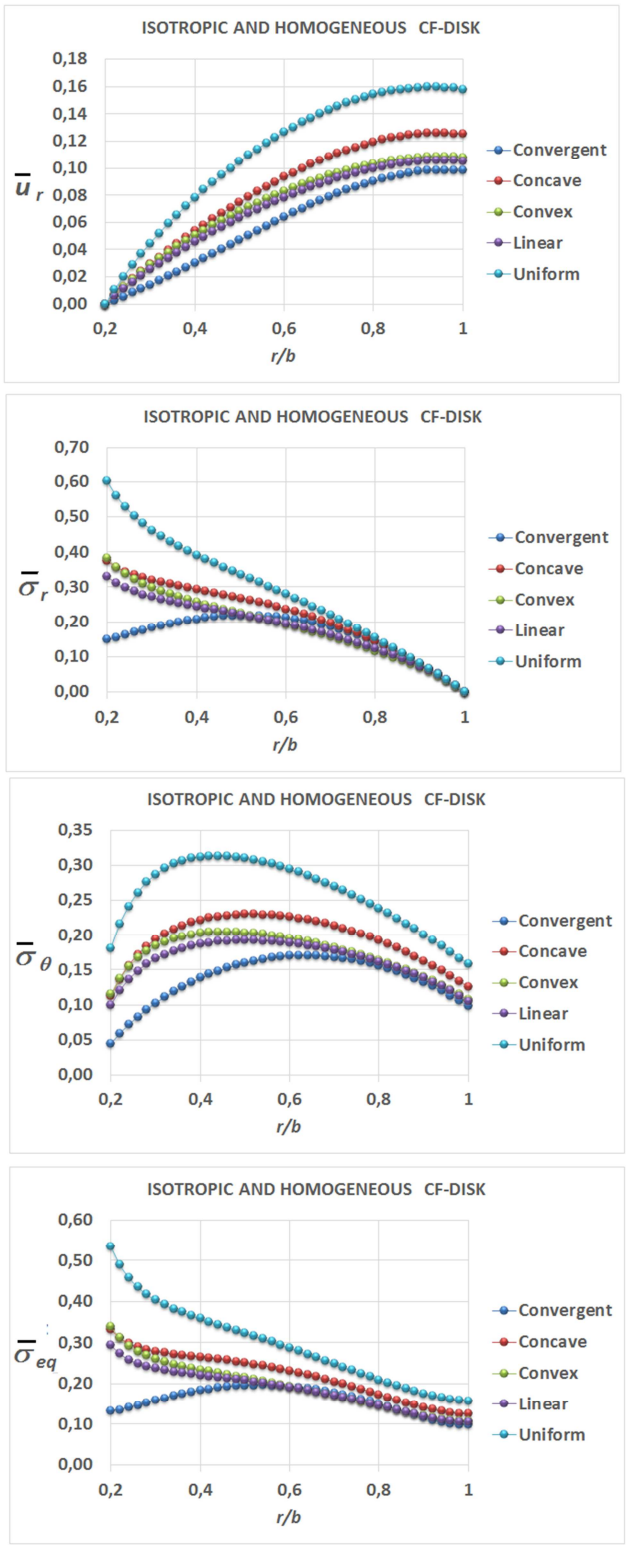

Figure 8. Elastic fields in a non-uniform CF-disk made of an isotropic and homogeneous material under centrifugal forces.

Figure 6 suggests that, E-FGM and V-VFG curves have smaller slopes towards the inner surface. That is both become rich in ceramic more slowly towards the outer surface than MT-FGM.

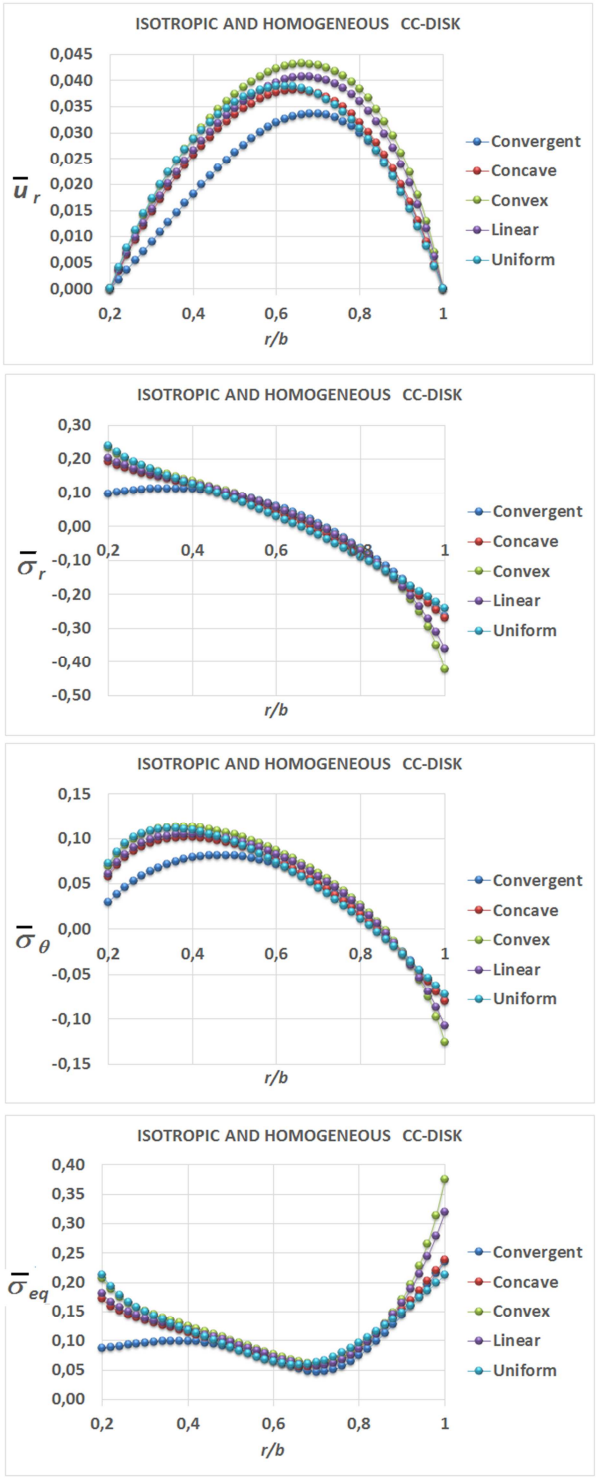

Figure 9. Elastic fields in a non-uniform CC-disk made of an isotropic and homogeneous material under centrifugal forces.

In S-FGM variation in Figure 6, ceramic-rich layers at both the inner and outer surfaces develop.

Figure 7 and Table 5 suggest that, for a traction-free rotating disk, a convergent hyperbolic profile is better than the others. A uniform disk profile offers the maximum equivalent stress which develops at the inner surface than the others. However, this situation turns reversely when the only pressure loads are concerned. In this case, a convergent hyperbolic profile becomes the worst while a uniform disk is the best (Table 6 and Figure 10).

For a mounted rotating CF-disk, from Table 7 and Figure 8, similar results of a FF- rotating disk are observed. That is a uniform profile is still the worst for a rotating CF-disk while a convergent hyperbolic one is the best.

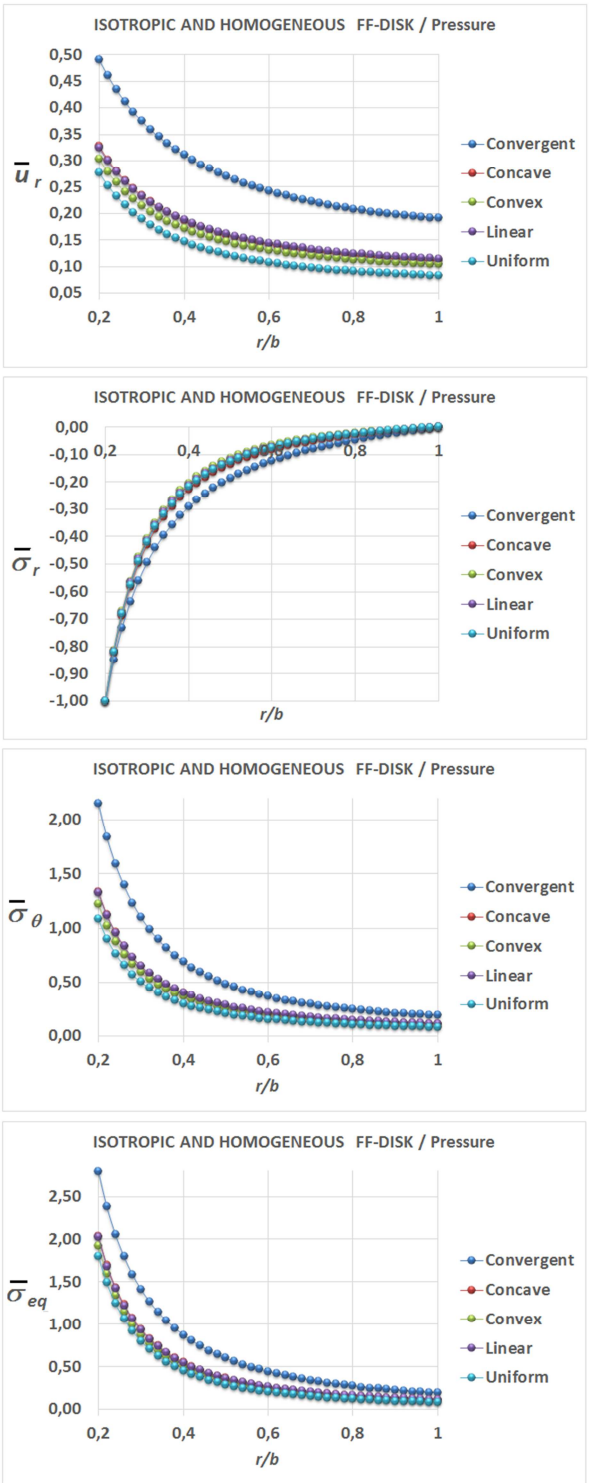

Figure 10. Elastic fields in a non-uniform FF-disk made of an isotropic and homogeneous material under pressure loads.

Table 8 and Figure 9, for a mounted and having casing rotating disk, it is seen that the radial and circumferential stresses in compression may develop under this boundary conditions. A convergent hyperbolic profile is still the best option among the others. A convex parabolic profile may be worse than the uniform thickness at some surfaces.

As a second examination, effects of the material grading rules (Figure 6) on the variation of elastic fields in a uniform disk are to be explored. Comparison of displacement and stresses in a uniform FF/CF/CC disc with different material grading rules under centrifugal and pressure loads is presented in Table 9. Figure 11 shows elastic field variations in uniform FGM disks under centrifugal forces.

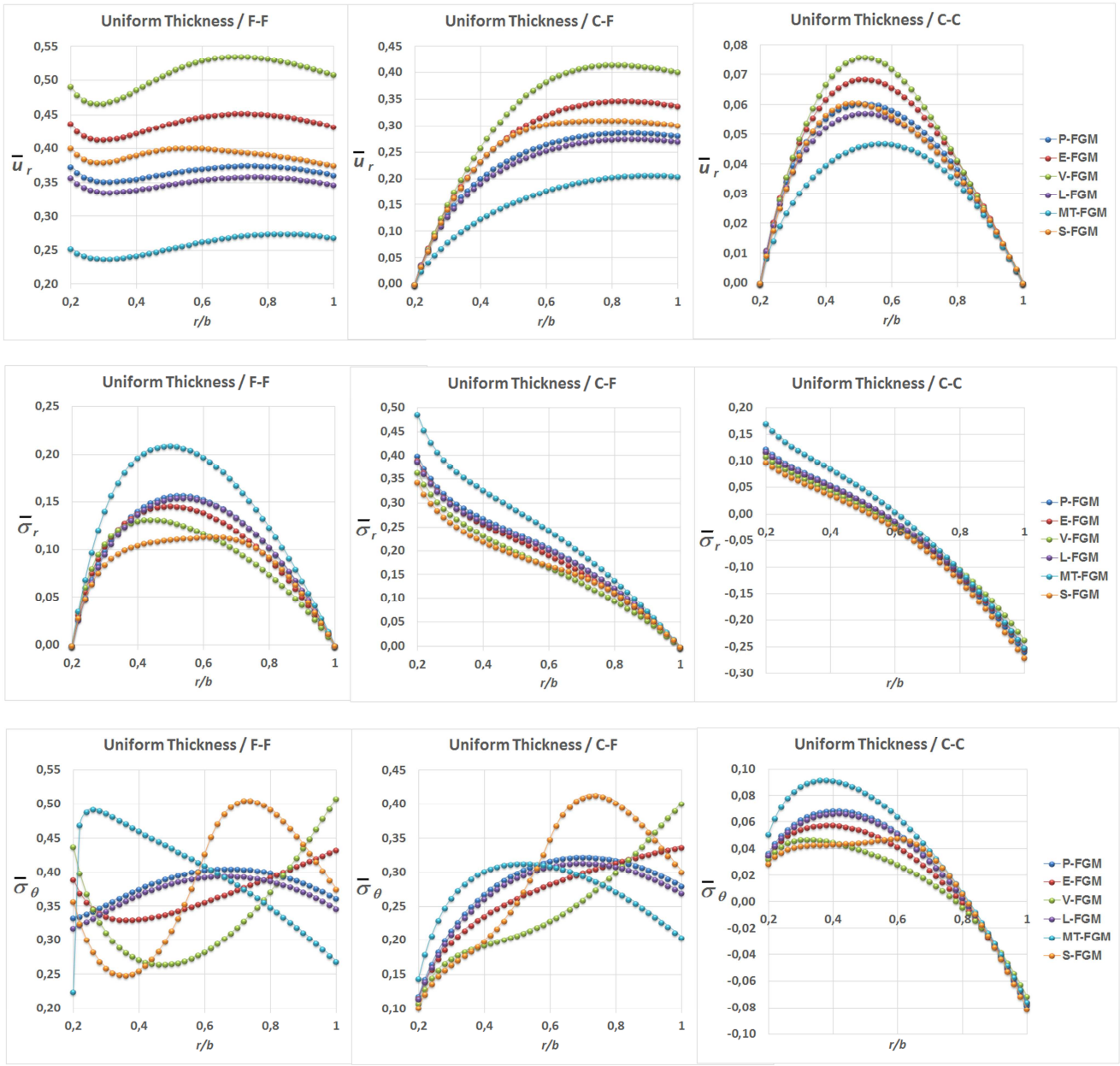

Figure 11. Elastic fields in uniform FGM disks under centrifugal forces.

From Table 9, MT-FGM seems the best for the maximum equivalent stress while V-FGM, S-FGM, and E-FGM are poorer under pressure loads. When only centrifugal forces are concerned, P-FGM is the best for FF-uniform-FGM disks, E-FGM is the best for CF-uniform-FGM disk, and V-FGM is the best for CC-uniform-FGM disk.

As a final examination, variable thickness FGM disks are considered. Some illustrations of the variation of the radial displacement, radial stress, circumferential stress and equivalent stress in FGM rotating disks are given in Figure 12 for certain disk profiles, boundary conditions and material grading rules. Comparisons of the equivalent stress variations

in non-uniform FGM FF/CF/CC disks under centrifugal forces are presented in Figure 13. Some numerical results are given in Tables 10-13.

From Figure 13 and Tables 10-13, the followings outcomes may be reached:

a. Both P-FGM and L-FGM offer almost uniform equivalent stress distribution for both FF and CF rotating disks (Figure 13).

b. The location of the maximum equivalent stress may change regarding to the boundary conditions and material grading rules employed.

c. For rotating CC-disks, the maximum equivalent stress build up at the outer surface. Under this boundary condition, the uniform profile with V-FGM offers the best option for the maximum equivalent stress. A parabolic-concave or a hyperbolic convergent disk may be second choices for a FGM rotating CC-disk.

d. For rotating FF and CF FGM disks, the maximum equivalent stress develops at different surfaces. Its location may be at the outer surface, or at a surface closer to the inner surface, or at an intermediate surface. S-FGM grading rule, in general, gives two intermediate locations for the maximum equivalent stress.

e. A MT-FGM grading rule may offer different locations such as the inner, the intermediate or the surface closer to the inner surface for the maximum equivalent stress regarding to the profile types and boundary conditions.

Table 9. Comparison of displacement and stresses in a uniform FF/CF/CC disc with different material grading rules under centrifugal and pressure loads.

r/b	**P-FGM**	**E-FGM**	**V-FGM**	**S-FGM**	**MT-FGM**	**P-FGM**	**E-FGM**	**V-FGM**	**S-FGM**	**MT-FGM**
	FREE-FREE (FF) – Centrifugal Forces					FREE-FREE (FF) – Pressure Loads				
	$\bar{u}_r$					$\bar{u}_r$				
0.2	0.374695	0.437615	0.492084	0.401685	0.253481	0.935888	1.119530	1.349135	1.168052	0.520886
0.4	0.356518	0.423596	0.487124	0.391635	0.243283	0.387894	0.486331	0.623446	0.458678	0.244799
0.6	0.371670	0.448139	0.529959	0.401405	0.263422	0.263768	0.323047	0.398906	0.280944	0.175263
0.8	0.375278	0.451404	0.532777	0.392174	0.275249	0.218880	0.264863	0.320515	0.233334	0.146011
1.	0.362252	0.433596	0.509185	0.376016	0.269302	0.199994	0.241632	0.291834	0.213508	0.130910
	$\bar{\sigma}_r$					$\bar{\sigma}_r$				
0.2	0.000000	0.000000	0.000000	0.000000	0.000000	-1.000000	-1.000000	-1.000000	-1.000000	-1.000000
0.4	0.141269	0.138149	0.130958	0.105358	0.196733	-0.319796	-0.305958	-0.283142	-0.335367	-0.270606
0.6	0.153180	0.139487	0.118053	0.113713	0.197500	-0.134995	-0.135812	-0.134103	-0.164883	-0.097821
0.8	0.102585	0.091124	0.074718	0.092630	0.124053	-0.049893	-0.054500	-0.059586	-0.059193	-0.031682
1.	0.000000	0.000000	0.000000	0.000000	0.000000	0.000000	0.000000	0.000000	0.000000	0.000000
	$\bar{\sigma}_\theta$					$\bar{\sigma}_\theta$				
0.2	0.333698	0.389733	0.438242	0.357734	0.225746	0.533488	0.697037	0.901520	0.740250	0.163893
0.4	0.376138	0.331794	0.271839	0.256293	0.461089	0.267192	0.241563	0.212689	0.162539	0.323392
0.6	0.404203	0.357066	0.283483	0.428199	0.410672	0.213745	0.186487	0.146492	0.226356	0.204465
0.8	0.400072	0.393903	0.371950	0.492825	0.349543	0.200423	0.198733	0.192402	0.258927	0.156175
1.	0.362252	0.433596	0.509185	0.376016	0.269302	0.199994	0.241632	0.291834	0.213508	0.130910
	$\bar{\sigma}_{eq}$					$\bar{\sigma}_{eq}$				
0.2	0.333698	0.389733	0.438242	0.357734	0.225746	1.348369	1.477463	1.647500	1.512686	1.091217
0.4	0.329090	0.288679	0.235472	0.223123	0.400743	0.509026	0.475259	0.430845	0.439773	0.515094
0.6	0.353452	0.311684	0.246644	0.384179	0.355738	0.304573	0.280267	0.243081	0.340214	0.267162
0.8	0.359917	0.357168	0.340790	0.453659	0.306933	0.229475	0.230860	0.228108	0.293043	0.174190
1.	0.362252	0.433596	0.509185	0.376016	0.269302	0.199994	0.241632	0.291834	0.213508	0.130910
	FIXED-FREE (CF) – Centrifugal Forces					FIXED-FIXED (CC) – Centrifugal Forces				
	$\bar{u}_r$					$\bar{u}_r$				
0.2	0.000000	0.000000	0.000000	0.000000	0.000000	0.000000	0.000000	0.000000	0.000000	0.000000
0.4	0.201220	0.233494	0.259728	0.233899	0.124156	0.055651	0.062004	0.066905	0.056750	0.039924
0.6	0.266067	0.321862	0.384462	0.304791	0.178133	0.058607	0.065999	0.072293	0.056515	0.047003
0.8	0.287647	0.347871	0.415872	0.311932	0.204195	0.038445	0.041067	0.041621	0.037028	0.034010
1.	0.282181	0.339144	0.402741	0.302592	0.205597	0.000000	0.000000	0.000000	0.000000	0.000000
	$\bar{\sigma}_r$					$\bar{\sigma}_r$				
0.2	0.400363	0.390892	0.364740	0.343893	0.486635	0.124211	0.117966	0.108918	0.098203	0.171427
0.4	0.269303	0.257746	0.234232	0.220689	0.328420	0.056173	0.051496	0.045004	0.037380	0.086179
0.6	0.207226	0.192575	0.166966	0.170415	0.245103	-0.013208	-0.015135	-0.016495	-0.024368	0.006018
0.8	0.122560	0.112428	0.096451	0.112987	0.139471	-0.115829	-0.112845	-0.103180	-0.124751	-0.104738
1.	0.000000	0.000000	0.000000	0.000000	0.000000	-0.258456	-0.252904	-0.236532	-0.268823	-0.250865
	$\bar{\sigma}_\theta$					$\bar{\sigma}_\theta$				
0.2	0.120109	0.117268	0.109422	0.103168	0.145990	0.037263	0.035390	0.032675	0.029461	0.051428
0.4	0.269164	0.237369	0.194263	0.200397	0.303715	0.068950	0.057949	0.045441	0.043772	0.091835

r/b	P-FGM	E-FGM	V-FGM	S-FGM	MT-FGM	P-FGM	E-FGM	V-FGM	S-FGM	MT-FGM
0.6	0.318627	0.284170	0.230052	0.350357	0.311172	0.052529	0.041883	0.028891	0.048174	0.064510
0.8	0.319830	0.316219	0.301773	0.403782	0.273543	0.003083	-0.000504	-0.003648	0.006482	0.007170
1.	0.282181	0.339144	0.402741	0.302592	0.205597	-0.077537	-0.075871	-0.070959	-0.080647	-0.075260
	$\overline{\sigma}_{eq}$					$\overline{\sigma}_{eq}$				
0.2	0.355851	0.347432	0.324188	0.305659	0.432530	0.110401	0.104851	0.096808	0.087284	0.152368
0.4	0.269234	0.248186	0.217025	0.211275	0.316791	0.063533	0.055007	0.045224	0.040952	0.089142
0.6	0.280068	0.251224	0.205890	0.303455	0.283962	0.060229	0.051158	0.039791	0.063940	0.061722
0.8	0.279489	0.277638	0.266952	0.360810	0.236911	0.117401	0.112593	0.101405	0.128115	0.108501
1.	0.282181	0.339144	0.402741	0.302592	0.205597	0.229720	0.224786	0.210234	0.238936	0.222974

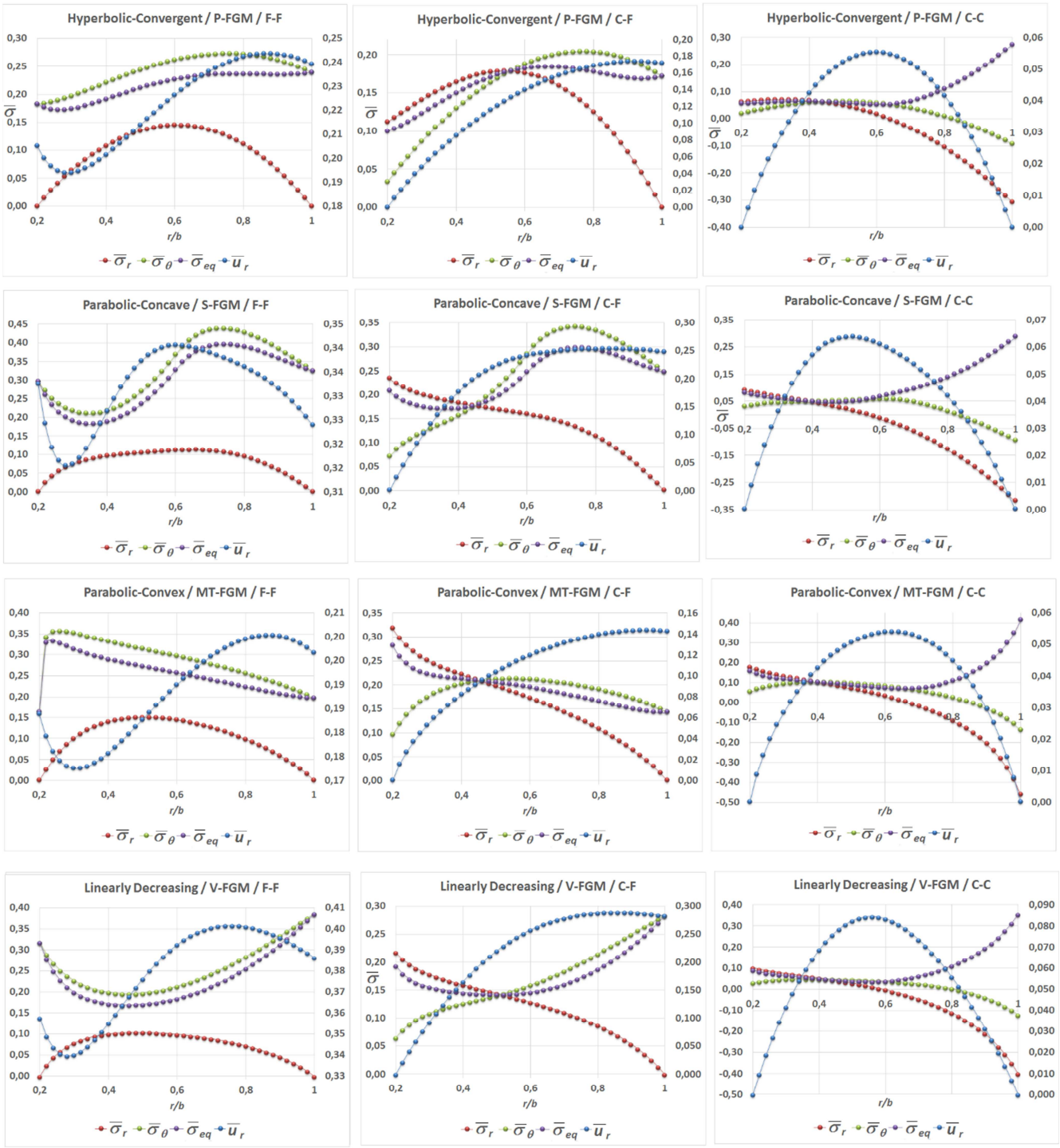

Figure 12. Variations of elastic fields in non-uniform FGM disks under centrifugal forces (the second axis is for $\overline{u}_r$)

f. A parabolic convex disk with MT-FGM seems to be the best option for FF disks under pressure (Table 13). As stated above (Figure 6), in the variation of MT-FGM grading rule with the inhomogeneity parameter less than unit ($n=0.25$), the curve has higher slopes towards the inner surface. This means that the mixture is much richer in ceramic than the others at each surface. This result may be obtained by using V-FGM with the similar inhomogeneity index value.

g. Generally speaking, it may be concluded that either a MT-FGM or V-FGM with inhomogeneity indexes which are smaller than the unit are preferable with parabolic convex FF disks subjected to the internal pressure.

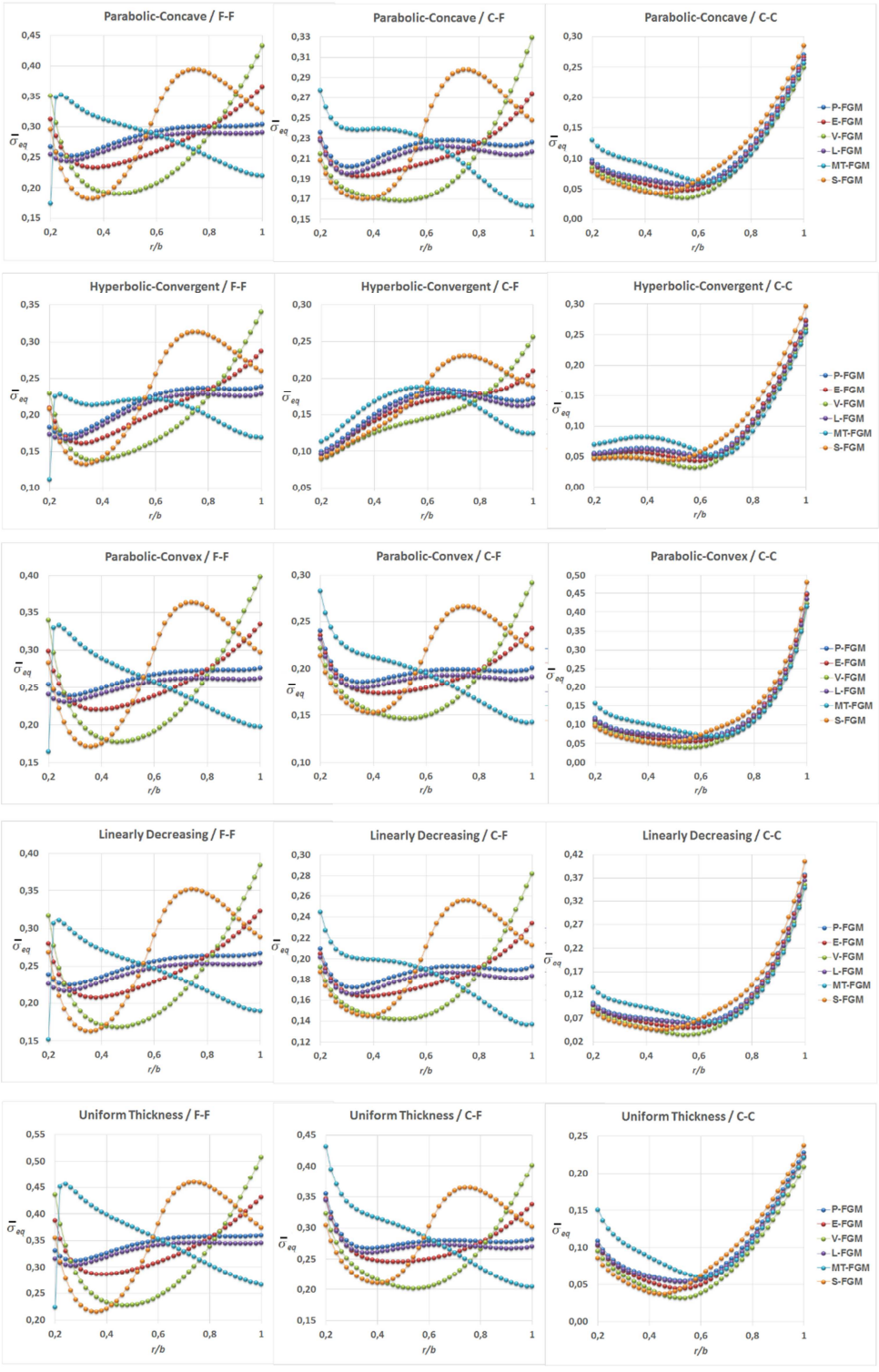

Figure 13. Comparisons of the equivalent stress variations in non-uniform FGM disks under centrifugal forces.

Table 10. Comparison of displacement and stresses in hyperbolically and linearly tapered discs with different material grading rules under centrifugal forces.

	HYPERBOLIC-CONVERGENT					**LINEARLY DECREASING**				
r/b	**P-FGM**	**E-FGM**	**V-FGM**	**S-FGM**	**MT-FGM**	**P-FGM**	**E-FGM**	**V-FGM**	**S-FGM**	**MT-FGM**
	FREE-FREE (FF)					FREE-FREE (FF)				
	$\bar{u}_r$					$\bar{u}_r$				
0.2	0.205103	0.234607	0.257213	0.233256	0.125951	0.269725	0.316291	0.357745	0.302765	0.172555
0.4	0.201447	0.236206	0.267254	0.237710	0.124971	0.256539	0.306492	0.355108	0.295575	0.165574
0.6	0.226268	0.273044	0.324822	0.263015	0.148368	0.269666	0.327993	0.392634	0.305514	0.181259
0.8	0.242254	0.292824	0.349616	0.267335	0.167784	0.275750	0.335134	0.401235	0.300737	0.192831
1.	0.239219	0.287318	0.340729	0.260562	0.169342	0.268553	0.324596	0.386410	0.290072	0.191118
	$\bar{\sigma}_r$					$\bar{\sigma}_r$				
0.2	0.000000	0.000000	0.000000	0.000000	0.000000	0.000000	0.000000	0.000000	0.000000	0.000000
0.4	0.107865	0.106646	0.101467	0.090548	0.136224	0.103831	0.103200	0.099516	0.082105	0.137006
0.6	0.144801	0.136414	0.120537	0.120351	0.172956	0.120915	0.112929	0.098612	0.094328	0.148559
0.8	0.111145	0.103489	0.090768	0.103582	0.126994	0.090693	0.083296	0.071472	0.083108	0.105289
1.	0.000000	0.000000	0.000000	0.000000	0.000000	0.000000	0.000000	0.000000	0.000000	0.000000
	$\bar{\sigma}_\theta$					$\bar{\sigma}_\theta$				
0.2	0.182662	0.208938	0.229070	0.207734	0.112170	0.240213	0.281684	0.318603	0.269638	0.153675
0.4	0.220946	0.193899	0.158026	0.163542	0.247403	0.271311	0.241041	0.199383	0.194206	0.314742
0.6	0.261537	0.232983	0.188206	0.294324	0.249818	0.296202	0.264588	0.213371	0.328242	0.286379
0.8	0.271737	0.268836	0.256600	0.348077	0.228484	0.298563	0.297137	0.284676	0.381544	0.250394
1.	0.239219	0.287318	0.340729	0.260562	0.169342	0.268553	0.324596	0.386410	0.290072	0.191118
	FIXED-FREE (CF)					FIXED-FREE (CF)				
	$\bar{u}_r$					$\bar{u}_r$				
0.2	0.000000	0.000000	0.000000	0.000000	0.000000	0.000000	0.000000	0.000000	0.000000	0.000000
0.4	0.085776	0.100390	0.113296	0.109075	0.049712	0.126346	0.147375	0.165453	0.153881	0.074769
0.6	0.139832	0.172780	0.213373	0.172698	0.090201	0.174060	0.212611	0.257834	0.208610	0.112325
0.8	0.168857	0.208390	0.257061	0.190611	0.118058	0.194140	0.237354	0.288381	0.218027	0.133826
1.	0.171998	0.210092	0.256214	0.190208	0.124642	0.193648	0.234950	0.283088	0.214079	0.137870
	$\bar{\sigma}_r$					$\bar{\sigma}_r$				
0.2	0.111978	0.108104	0.100433	0.101732	0.127854	0.236872	0.231569	0.217359	0.211849	0.276384
0.4	0.164539	0.156627	0.141548	0.144785	0.186692	0.181474	0.174457	0.159541	0.155675	0.211571
0.6	0.176378	0.166053	0.146370	0.158297	0.195025	0.155299	0.146308	0.128941	0.134532	0.175493
0.8	0.125431	0.118253	0.105311	0.120285	0.134935	0.104797	0.098396	0.087038	0.099176	0.114175
1.	0.000000	0.000000	0.000000	0.000000	0.000000	0.000000	0.000000	0.000000	0.000000	0.000000
	$\bar{\sigma}_\theta$					$\bar{\sigma}_\theta$				
0.2	0.033593	0.032431	0.030130	0.030519	0.038356	0.071062	0.069471	0.065208	0.063555	0.082915
0.4	0.129662	0.115799	0.096551	0.106013	0.138165	0.172722	0.153354	0.126849	0.134986	0.187040
0.6	0.187696	0.171349	0.143788	0.217038	0.178842	0.214364	0.193443	0.159371	0.245166	0.202496
0.8	0.203796	0.204700	0.200241	0.262111	0.174442	0.222485	0.222264	0.215307	0.288287	0.186106
1.	0.171998	0.210092	0.256214	0.190208	0.124642	0.193648	0.234950	0.283088	0.214079	0.137870
	FIXED-FIXED (CC)					FIXED-FIXED (CC)				
	$\bar{u}_r$					$\bar{u}_r$				
0.2	0.000000	0.000000	0.000000	0.000000	0.000000	0.000000	0.000000	0.000000	0.000000	0.000000
0.4	0.042492	0.047584	0.051418	0.047638	0.027573	0.057850	0.064274	0.068772	0.062069	0.039198
0.6	0.055402	0.063496	0.070999	0.058543	0.041047	0.067026	0.075875	0.083466	0.068768	0.050730
0.8	0.041653	0.045382	0.047091	0.042463	0.034700	0.050184	0.054277	0.055797	0.050532	0.041962
1.	0.000000	0.000000	0.000000	0.000000	0.000000	0.000000	0.000000	0.000000	0.000000	0.000000
	$\bar{\sigma}_r$					$\bar{\sigma}_r$				
0.2	0.063001	0.059217	0.054060	0.052966	0.078751	0.118277	0.111523	0.101700	0.096684	0.155080
0.4	0.067115	0.060704	0.051825	0.049892	0.089280	0.068762	0.062531	0.053785	0.049545	0.096709
0.6	0.016686	0.010820	0.003909	-0.00022	0.039355	0.007914	0.003045	-0.002354	-0.007352	0.030864
0.8	-0.10521	-0.10672	-0.10218	-0.12413	-0.08385	-0.115300	-0.116028	-0.110030	-0.131764	-0.093715
1.	-0.30832	-0.30641	-0.29118	-0.33358	-0.28548	-0.427049	-0.423549	-0.400466	-0.458832	-0.393135
	$\bar{\sigma}_\theta$					$\bar{\sigma}_\theta$				
0.2	0.018900	0.017765	0.016218	0.015890	0.023625	0.035483	0.033457	0.030510	0.029005	0.046524
0.4	0.059914	0.050827	0.040094	0.042298	0.072354	0.074786	0.062815	0.048967	0.050473	0.093795
0.6	0.058407	0.047909	0.034407	0.057408	0.066566	0.066980	0.054284	0.038363	0.065309	0.076936
0.8	0.009427	0.004837	0.000240	0.013115	0.014220	0.014795	0.009268	0.003597	0.020392	0.019501
1.	-0.09250	-0.09192	-0.08735	-0.10007	-0.08564	-0.128115	-0.127065	-0.120140	-0.137650	-0.117940

Table 11. Comparison of displacement and stresses in parabolically tapered discs with different material grading rules under centrifugal forces.

	PARABOLIC-CONCAVE					**PARABOLIC-CONVEX**				
r/b	**P-FGM**	**E-FGM**	**V-FGM**	**S-FGM**	**MT-FGM**	**P-FGM**	**E-FGM**	**V-FGM**	**S-FGM**	**MT-FGM**
	FREE-FREE (FF)					FREE-FREE (FF)				
	$\bar{u}_r$					$\bar{u}_r$				
0.2	0.300511	0.350789	0.394099	0.332399	0.194955	0.284329	0.334666	0.380370	0.316839	0.183799
0.4	0.287537	0.342061	0.393848	0.326745	0.188236	0.269418	0.322838	0.375513	0.307729	0.175670
0.6	0.304812	0.369253	0.439655	0.340500	0.208164	0.280382	0.341512	0.409336	0.314913	0.189938
0.8	0.312745	0.378375	0.450369	0.336071	0.222401	0.284053	0.345607	0.414058	0.308062	0.199517
1.	0.304138	0.365946	0.433113	0.323882	0.219939	0.275597	0.333593	0.397537	0.296318	0.196687
	$\bar{\sigma}_r$					$\bar{\sigma}_r$				
0.2	0.000000	0.000000	0.000000	0.000000	0.000000	0.000000	0.000000	0.000000	0.000000	0.000000
0.4	0.121941	0.120373	0.115101	0.095240	0.162993	0.104456	0.103879	0.100352	0.081339	0.139318
0.6	0.142893	0.132384	0.114570	0.110488	0.178020	0.116334	0.108399	0.094304	0.089305	0.144050
0.8	0.103163	0.093741	0.079395	0.093998	0.121426	0.084428	0.077258	0.065846	0.077091	0.098478
1.	0.000000	0.000000	0.000000	0.000000	0.000000	0.000000	0.000000	0.000000	0.000000	0.000000
	$\bar{\sigma}_\theta$					$\bar{\sigma}_\theta$				
0.2	0.267630	0.312407	0.350978	0.296030	0.173624	0.253219	0.298049	0.338752	0.282172	0.163688
0.4	0.305762	0.270574	0.222552	0.216029	0.359992	0.283554	0.252450	0.209375	0.200949	0.332121
0.6	0.336673	0.299447	0.240168	0.367437	0.331110	0.305157	0.272739	0.219896	0.335962	0.296605
0.8	0.338710	0.335384	0.319288	0.426710	0.288787	0.304854	0.303830	0.291401	0.388425	0.255937
1.	0.304138	0.365946	0.433113	0.323882	0.219939	0.275597	0.333593	0.397537	0.296318	0.196687
	FIXED-FREE (CF)					FIXED-FREE (CF)				
	$\bar{u}_r$					$\bar{u}_r$				
0.2	0.000000	0.000000	0.000000	0.000000	0.000000	0.000000	0.000000	0.000000	0.000000	0.000000
0.4	0.145781	0.169787	0.190015	0.175927	0.087128	0.137561	0.160519	0.180202	0.165801	0.081970
0.6	0.203406	0.248074	0.300101	0.241150	0.132882	0.184262	0.224707	0.271633	0.218916	0.119261
0.8	0.227362	0.277319	0.335851	0.252381	0.158747	0.201919	0.246488	0.298569	0.226056	0.139018
1.	0.225990	0.273581	0.328625	0.247184	0.162658	0.200142	0.242629	0.291686	0.220908	0.142058
	$\bar{\sigma}_r$					$\bar{\sigma}_r$				
0.2	0.264619	0.257959	0.240927	0.233941	0.311582	0.269763	0.264474	0.248855	0.239796	0.316975
0.4	0.215279	0.206243	0.187719	0.182494	0.253624	0.187827	0.180957	0.165892	0.159773	0.220751
0.6	0.185931	0.174249	0.152677	0.158957	0.212782	0.151182	0.142404	0.125407	0.129505	0.172041
0.8	0.120641	0.112349	0.098372	0.113130	0.133418	0.098007	0.091865	0.081006	0.092368	0.107239
1.	0.000000	0.000000	0.000000	0.000000	0.000000	0.000000	0.000000	0.000000	0.000000	0.000000
	$\bar{\sigma}_\theta$					$\bar{\sigma}_\theta$				
0.2	0.079386	0.077388	0.072278	0.070182	0.093475	0.080929	0.079342	0.074656	0.071939	0.095092
0.4	0.201058	0.178251	0.147028	0.155680	0.220081	0.185127	0.164313	0.135796	0.143054	0.201696
0.6	0.251840	0.226770	0.186277	0.284440	0.241108	0.222963	0.200779	0.164770	0.253775	0.210714
0.8	0.259931	0.258903	0.249851	0.333210	0.220157	0.228103	0.227722	0.220181	0.295765	0.189916
1.	0.225990	0.273581	0.328625	0.247184	0.162658	0.200142	0.242629	0.291686	0.220908	0.142058
	FIXED-FIXED (CC)					FIXED-FIXED (CC)				
	$\bar{u}_r$					$\bar{u}_r$				
0.2	0.000000	0.000000	0.000000	0.000000	0.000000	0.000000	0.000000	0.000000	0.000000	0.000000
0.4	0.053898	0.059988	0.064478	0.056778	0.037176	0.061853	0.068565	0.073141	0.065826	0.042433
0.6	0.060793	0.068746	0.075623	0.060725	0.047091	0.070504	0.079539	0.087088	0.071960	0.053803
0.8	0.042376	0.045562	0.046522	0.041765	0.036417	0.053339	0.057575	0.059037	0.053591	0.044747
1.	0.000000	0.000000	0.000000	0.000000	0.000000	0.000000	0.000000	0.000000	0.000000	0.000000
	$\bar{\sigma}_r$					$\bar{\sigma}_r$				
0.2	0.109091	0.103038	0.094388	0.088057	0.145044	0.131467	0.123906	0.112837	0.106828	0.174620
0.4	0.062976	0.057367	0.049575	0.043904	0.091141	0.070173	0.063758	0.054789	0.050264	0.100121
0.6	-0.00156	-0.00513	-0.00871	-0.01567	0.020313	0.007031	0.002147	-0.003177	-0.007841	0.030195
0.8	-0.11669	-0.11534	-0.10722	-0.13002	-0.09998	-0.114841	-0.115659	-0.109707	-0.130263	-0.093588
1.	-0.30284	-0.29794	-0.27988	-0.32015	-0.28704	-0.504453	-0.500617	-0.473130	-0.540796	-0.463666
	$\bar{\sigma}_\theta$					$\bar{\sigma}_\theta$				
0.2	0.032727	0.030911	0.028316	0.026417	0.043513	0.039440	0.037172	0.033851	0.032048	0.052386
0.4	0.069350	0.058328	0.045654	0.045746	0.088782	0.078956	0.066124	0.051354	0.052845	0.100165
0.6	0.058130	0.046818	0.032784	0.054915	0.068916	0.070067	0.056591	0.039812	0.068295	0.080835
0.8	0.006693	0.002397	-0.00164	0.010517	0.011327	0.018037	0.012056	0.005820	0.024469	0.022698
1.	-0.09085	-0.08938	-0.08396	-0.09605	-0.08611	-0.151336	-0.150185	-0.141939	-0.162239	-0.139100

Table 12. Comparison of displacement and stresses in a nonuniform L-FGM disc under centrifugal and pressure forces.

r/b	**HYP**	**PAR-I**	**PAR-II**	**LIN**	**UNI**	**HYP**	**PAR-I**	**PAR-II**	**LIN**	**UNI**
	FREE-FREE (FF) – Centrifugal Forces					FREE-FREE (FF) – Pressure Loads				
	$\bar{u}_r$					$\bar{u}_r$				
0.2	0.194860	0.285988	0.269558	0.255761	0.357936	1.804724	1.118597	1.038022	1.121427	0.922042
0.4	0.190970	0.273261	0.255056	0.242891	0.340187	1.016754	0.526879	0.480515	0.540394	0.381572
0.6	0.214679	0.289980	0.265673	0.255555	0.355018	0.760651	0.377500	0.350737	0.397329	0.260018
0.8	0.230725	0.298432	0.269912	0.262116	0.359405	0.646209	0.318024	0.299826	0.339305	0.215913
1.	0.228395	0.290770	0.262373	0.255798	0.347465	0.591870	0.291096	0.275457	0.311442	0.197297
	$\bar{\sigma}_r$					$\bar{\sigma}_r$				
0.2	0.000000	0.000000	0.000000	0.000000	0.000000	-1.000000	-1.000000	-1.000000	-1.000000	-1.000000
0.4	0.104084	0.118287	0.100875	0.100258	0.137744	-0.507520	-0.353168	-0.309460	-0.328269	-0.320043
0.6	0.141994	0.140811	0.114230	0.118715	0.151623	-0.281029	-0.161973	-0.128652	-0.144562	-0.134463
0.8	0.110799	0.103332	0.084393	0.090623	0.103152	-0.126407	-0.065417	-0.049836	-0.058946	-0.049450
1.	0.000000	0.000000	0.000000	0.000000	0.000000	0.000000	0.000000	0.000000	0.000000	0.000000
	$\bar{\sigma}_\theta$					$\bar{\sigma}_\theta$				
0.2	0.173539	0.254697	0.240064	0.227777	0.318772	1.307261	0.696206	0.624447	0.698727	0.521157
0.4	0.214360	0.297535	0.274854	0.263003	0.367552	0.822780	0.399311	0.367961	0.419741	0.269903
0.6	0.253362	0.326935	0.295097	0.286509	0.394031	0.662472	0.322024	0.305746	0.346715	0.214937
0.8	0.262387	0.327391	0.293384	0.287511	0.387893	0.603868	0.296224	0.282825	0.319301	0.199601
1.	0.228395	0.290770	0.262373	0.255798	0.347465	0.591870	0.291096	0.275457	0.311442	0.197297
	$\bar{\sigma}_{eq}$					$\bar{\sigma}_{eq}$				
0.2	0.173539	0.254697	0.240064	0.227777	0.318772	2.004044	1.476790	1.419289	1.478833	1.338940
0.4	0.185667	0.259470	0.240820	0.229900	0.321621	1.162807	0.652074	0.587393	0.649408	0.511522
0.6	0.219952	0.284039	0.257725	0.249335	0.344247	0.839059	0.426725	0.386480	0.437300	0.305253
0.8	0.228147	0.289884	0.261604	0.254597	0.347979	0.675994	0.333775	0.310754	0.352490	0.228377
1.	0.228395	0.290770	0.262373	0.255798	0.347465	0.591870	0.291096	0.275457	0.311442	0.197297
	FIXED-FREE (CF) – Centrifugal Forces					FIXED-FIXED (CC) – Centrifugal Forces				
	$\bar{u}_r$					$\bar{u}_r$				
0.2	0.000000	0.000000	0.000000	0.000000	0.000000	0.000000	0.000000	0.000000	0.000000	0.000000
0.4	0.081189	0.138556	0.130274	0.119645	0.192062	0.039997	0.050858	0.058376	0.054560	0.052584
0.6	0.132550	0.193466	0.174592	0.164937	0.254080	0.052315	0.057552	0.066719	0.063387	0.055584
0.8	0.160953	0.217124	0.192052	0.184732	0.275588	0.039759	0.040529	0.050916	0.047895	0.036850
1.	0.164490	0.216346	0.190842	0.184768	0.270875	0.000000	0.000000	0.000000	0.000000	0.000000
	$\bar{\sigma}_r$					$\bar{\sigma}_r$				
0.2	0.107972	0.255666	0.259684	0.228067	0.388199	0.060525	0.104764	0.126212	0.113520	0.119348
0.4	0.158882	0.208580	0.181237	0.175125	0.261984	0.064399	0.060584	0.067504	0.066094	0.054141
0.6	0.172338	0.182222	0.147639	0.151685	0.203821	0.017421	-0.000083	0.008192	0.009021	-0.011320
0.8	0.124447	0.120057	0.097335	0.104066	0.122349	-0.099117	-0.110464	-0.108358	-0.108778	-0.110002
1.	0.000000	0.000000	0.000000	0.000000	0.000000	-0.298490	-0.293632	-0.486878	-0.412457	-0.251288
	$\bar{\sigma}_\theta$					$\bar{\sigma}_\theta$				
0.2	0.032392	0.076700	0.077905	0.068420	0.116460	0.018158	0.031429	0.037864	0.034056	0.035804
0.4	0.125523	0.195445	0.179300	0.167274	0.262776	0.057676	0.066946	0.076232	0.072150	0.066668
0.6	0.181834	0.244604	0.215700	0.207435	0.310593	0.056587	0.056478	0.067960	0.064938	0.051174
0.8	0.197186	0.251657	0.219939	0.214689	0.310408	0.009752	0.007113	0.018060	0.014934	0.003598
1.	0.164490	0.216346	0.190842	0.184768	0.270875	-0.089547	-0.088090	-0.146063	-0.123737	-0.075386
	$\bar{\sigma}_{eq}$					$\bar{\sigma}_{eq}$				
0.2	0.095968	0.227241	0.230812	0.202711	0.345039	0.053796	0.093117	0.112179	0.100899	0.106079
0.4	0.145108	0.202333	0.180276	0.171334	0.262381	0.061314	0.064003	0.072264	0.069320	0.061371
0.6	0.177277	0.220145	0.190992	0.185937	0.273323	0.050198	0.056519	0.064257	0.060930	0.057673
0.8	0.172714	0.218018	0.190891	0.185955	0.270822	0.104335	0.114187	0.118426	0.116962	0.111844
1.	0.164490	0.216346	0.190842	0.184768	0.270875	0.265304	0.260986	0.432746	0.366600	0.223350

Table 13. Comparison of displacement and stresses in variable-thickness FF-discs with different material grading rules under pressure forces.

r/b	**P-FGM**	**E-FGM**	**V-FGM**	**S-FGM**	**MT-FGM**	**P-FGM**	**E-FGM**	**V-FGM**	**S-FGM**	**MT-FGM**
	HYPERBOLIC-CONVERGENT					LINEARLY VARYING				
	$\bar{u}_r$					$\bar{u}_r$				
0.2	1.831633	2.170212	2.561047	2.292851	0.985115	1.138693	1.365862	1.645870	1.429155	0.624330
0.4	1.032978	1.256357	1.532948	1.264460	0.588628	0.549636	0.687127	0.872541	0.668844	0.328548
0.6	0.771897	0.927478	1.109693	0.887799	0.454942	0.403618	0.498263	0.620173	0.457420	0.249416
0.8	0.655456	0.781048	0.921569	0.754171	0.388927	0.344532	0.422254	0.519205	0.390421	0.213491
1.	0.600304	0.714378	0.841515	0.691563	0.349618	0.316224	0.387125	0.475348	0.358714	0.192660
	$\bar{\sigma}_r$					$\bar{\sigma}_r$				
0.2	-1.00000	-1.00000	-1.00000	-1.00000	-1.00000	-1.000000	-1.000000	-1.000000	-1.000000	-1.000000
0.4	-0.50613	-0.46235	-0.39909	-0.53313	-0.39473	-0.327784	-0.307716	-0.276153	-0.347277	-0.269785
0.6	-0.28199	-0.27417	-0.25722	-0.37300	-0.17261	-0.145158	-0.144144	-0.139534	-0.189773	-0.097451
0.8	-0.12758	-0.13657	-0.14480	-0.16418	-0.06212	-0.059543	-0.065206	-0.071616	-0.075851	-0.032152

r/b	P-FGM	E-FGM	V-FGM	S-FGM	MT-FGM	P-FGM	E-FGM	V-FGM	S-FGM	MT-FGM
1.	0.000000	0.000000	0.000000	0.000000	0.000000	0.000000	0.000000	0.000000	0.000000	0.000000
	$\bar{\sigma}_\theta$					$\bar{\sigma}_\theta$				
0.2	1.331226	1.632759	1.980831	1.741979	0.577329	0.714103	0.916417	1.165787	0.972784	0.256019
0.4	0.815193	0.722453	0.612099	0.565496	0.854393	0.416211	0.378669	0.333703	0.279541	0.462048
0.6	0.659427	0.570135	0.442266	0.759709	0.555138	0.345496	0.307234	0.248435	0.392147	0.303501
0.8	0.606735	0.593284	0.561166	0.845034	0.422683	0.321178	0.323332	0.319146	0.440202	0.232604
1.	0.600304	0.714378	0.841515	0.691563	0.349618	0.316224	0.387125	0.475348	0.358714	0.192660
	$\bar{\sigma}_{eq}$					$\bar{\sigma}_{eq}$				
0.2	2.025682	2.301882	2.627646	2.403429	1.382258	1.491324	1.660192	1.877458	1.708536	1.149593
0.4	1.154683	1.034274	0.882166	0.951577	1.105916	0.645834	0.595485	0.528934	0.543895	0.641035
0.6	0.836847	0.746015	0.612800	0.999830	0.658631	0.436566	0.399320	0.340375	0.514015	0.362196
0.8	0.679568	0.672058	0.645856	0.937965	0.456918	0.354718	0.360387	0.360331	0.482619	0.250234
1.	0.600304	0.714378	0.841515	0.691563	0.349618	0.316224	0.387125	0.475348	0.358714	0.192660
	PARABOLIC-CONCAVE					PARABOLIC-CONVEX				
	$\bar{u}_r$					$\bar{u}_r$				
0.2	1.135635	1.359861	1.635759	1.420872	0.625695	1.053994	1.265401	1.528483	1.321288	0.579853
0.4	0.535698	0.667834	0.846034	0.644683	0.324501	0.488786	0.613741	0.784838	0.591870	0.295605
0.6	0.383215	0.469761	0.579240	0.424678	0.241613	0.356310	0.441652	0.553348	0.400329	0.222974
0.8	0.322664	0.391753	0.475324	0.357744	0.204291	0.304467	0.374775	0.464082	0.341985	0.190863
1.	0.295325	0.358060	0.433691	0.327852	0.183842	0.279708	0.343942	0.425356	0.314476	0.172346
	$\bar{\sigma}_r$					$\bar{\sigma}_r$				
0.2	-1.00000	-1.00000	-1.00000	-1.00000	-1.00000	-1.000000	-1.000000	-1.000000	-1.000000	-1.000000
0.4	-0.35273	-0.33288	-0.30141	-0.37298	-0.29087	-0.309055	-0.291439	-0.263367	-0.327086	-0.256907
0.6	-0.16264	-0.16230	-0.15817	-0.20718	-0.11157	-0.129179	-0.128577	-0.124986	-0.167641	-0.088307
0.8	-0.06605	-0.07214	-0.07877	-0.08178	-0.03849	-0.050339	-0.055231	-0.060919	-0.063711	-0.027639
1.	0.000000	0.000000	0.000000	0.000000	0.000000	0.000000	0.000000	0.000000	0.000000	0.000000
	$\bar{\sigma}_\theta$					$\bar{\sigma}_\theta$				
0.2	0.711380	0.911072	1.156783	0.965407	0.257235	0.638672	0.826948	1.061245	0.876719	0.216408
0.4	0.395679	0.357896	0.313471	0.257970	0.449033	0.364864	0.333251	0.295670	0.241437	0.411468
0.6	0.320585	0.281741	0.223684	0.354778	0.288856	0.304690	0.272085	0.221519	0.342736	0.270968
0.8	0.297707	0.296485	0.288211	0.399675	0.220264	0.284513	0.287769	0.286191	0.386409	0.208282
1.	0.295325	0.358060	0.433691	0.327852	0.183842	0.279708	0.343942	0.425356	0.314476	0.172346
	$\bar{\sigma}_{eq}$					$\bar{\sigma}_{eq}$				
0.2	1.489107	1.655634	1.869473	1.702181	1.150393	1.430585	1.584547	1.785353	1.626455	1.123940
0.4	0.648495	0.598361	0.532537	0.549432	0.645640	0.584298	0.541401	0.484409	0.494214	0.583966
0.6	0.425872	0.389156	0.332314	0.492237	0.357927	0.385853	0.354324	0.303939	0.450587	0.324269
0.8	0.335641	0.338369	0.334622	0.446221	0.241816	0.312736	0.318991	0.321015	0.421888	0.223388
1.	0.295325	0.358060	0.433691	0.327852	0.183842	0.279708	0.343942	0.425356	0.314476	0.172346

h. Both L-FGM and P-FGM seem to be the best for both FF and CF disks with any profile under centrifugal forces since they offer more smooth equivalent stresses. For a CC disk, V-FGM is the best under rotation (Figure 13).

i. Among the disk profiles the hyperbolic convergent ones exhibit best performance under centrifugal forces.

6. Conclusions

A comprehensive and accurate stress and displacement analysis of pressurized/rotating variable thickness disks made of arbitrarily functionally graded a metal and a ceramic is performed with the help of the transfer matrix approach under different boundary conditions. Some findings which may be very useful in the design of such disks are achieved:

a. Either a MT-FGM or a V-FGM grading rule having inhomogeneity indexes which are smaller than the unit are preferable with parabolic convex FF disks subjected to the internal pressure loads.

b. For rotating CC FGM disks, a uniform profile with either V-FGM or MT-FGM grading rules having inhomogeneity indexes much greater than the unit may be the best option for the maximum equivalent stress. A parabolic-concave or a hyperbolic convergent disk may be second choices for a FGM CC-disk under centrifugal forces.

c. A convergent hyperbolic profile becomes the worst while a uniform profile is the best for pressurized FF-disks made of a homogeneous and isotropic material.

d. When centrifugal forces are concerned, either L-FGM or P-FGM may be better solution for non-uniform FGM rotating disks.

e. For centrifugal forces, the convergent hyperbolic disk profiles seem to be the best solution.

It is worth noting that, varying inhomogeneity indexes in both S-FGM, MT-FGM, and V-FGM may offer different results. In general, a mixture having mostly ceramic at each surface may be preferred to get minimum equivalent stresses for a disk under pressure forces.

References

[1] Güven U. 1995. Tresca's yield condition and the linear hardening rotating solid disk of variable thickness, Zeitschrift fur Angewandte Mathematik und Mechanik, 75, pp. 805-807.

[2] Eraslan A. N. 2003. Elastoplastic deformations of rotating parabolic solid disks using Tresca's yield criterion, European Journal of Mechanics A/Solids, 22, pp. 861-874.

[3] Eraslan A. N. 2003. Elastic–plastic deformations of rotating variable thickness annular disks with free, pressurized and radially constrained boundary conditions, Int J Mech Sci, 45, pp. 643-667.

[4] Apatay T., and Eraslan A. N. 2003. Elastic deformation of rotating parabolic discs: analytical solutions (in Turkish), Journal of the Faculty of Engineering and Architecture of Gazi University, 18, pp. 115-135.

[5] Calderale P. M., Vivio F., and Vullo V. 2012. Thermal stresses of rotating hyperbolic disks as particular case of non-linearly variable thickness disks, Journal of Thermal Stresses, 35, pp. 877-891.

[6] Vivio F., Vullo V., and Cifani P. 2014. Theoretical stress analysis of rotating hyperbolic disk without singularities subjected to thermal load, Journal of Thermal Stresses, 37, pp. 117-136.

[7] Eraslan A. N., and Ciftci B. 2015. Analytical and numerical solutions to rotating variable thickness disks for a new thickness profile, Journal of Multidisciplinary Engineering Science and Technology (JMEST), 2 (9), pp. 2359-2364.

[8] Argeso H. 2012. Analytical solutions to variable thickness and variable material property rotating disks for a new three-parameter variation function, Mechanics Based Design of Structures and Machines, 40, pp. 133-152.

[9] Murthy D., and Sherbourne A. 1970. Elastic stresses in anisotropic discs of variable thickness. Int J Mech Sci, 12, pp. 627-640.

[10] Reddy T. Y., and Srinath H. 1974. Elastic stresses in a rotating anisotropic annular disc of variable thickness and variable density, Int J Mech Sci, 16 (2), pp. 85-89.

[11] Gurushankar G. V. 1975. Thermal stresses in a rotating nonhomogeneous, anisotropic disc of varying thickness and density, The Journal of Strain Analysis for Engineering Design, 10, pp. 137-142.

[12] Zenkour A. M., and Allam N. M. N. 2006. On the rotating fiber-reinforced viscoelastic composite solid and annular disks of variable thickness, International Journal of Computational Methods in Engineering Science and Mechanics, 7, pp. 21-31.

[13] Eraslan A. N., Kaya Y., and Varlı E. 2016. Analytical solutions to orthotropic variable thickness disk problems, Pamukkale University Journal of Engineering Sciences, 22 (1), pp. 24-30.

[14] Kacar I., Yıldırım V. 2017. Effect of the anisotropy ratios on the exact elastic behavior of functionally power-graded polar orthotropic rotating uniform discs under various boundary conditions, Digital Proceeding of ICOCEE – Cappadocia 2017, Nevsehir, Turkey, pp. 1743-1752.

[15] Essa S., and Argeso H. 2017. Elastic analysis of variable profile and polar orthotropic FGM rotating disks for a variation function with three parameters, Acta Mechanica, 228, pp. 3877–3899.

[16] Zheng Y., Bahaloo H., Mousanezhad D., Vaziri A., and Nayeb-Hashemi H. 2017. Displacement and stress fields in a functionally graded fiber-reinforced rotating disk with nonuniform thickness and variable angular velocity, Journal of Engineering Materials and Technology, 39, 031010-1-9.

[17] Yıldırım V. 2018. Unified exact solutions to the hyperbolically tapered pressurized/rotating disks made of nonhomogeneous isotropic/orthotropic materials, International Journal of Advanced Materials Research (to be published)

[18] Eraslan, A. N. and Akiş, T. 2006. On the plane strain and plane stress solutions of functionally graded rotating solid shaft and solid disk problems, Acta Mechanica, 181 (1–2), pp. 43–63.

[19] Vivio F., and Vullo V. 2007. Elastic stress analysis of rotating converging conical disks subjected to thermal load and having variable density along the radius, International Journal of Solids and Structures, 44, pp. 7767–7784.

[20] Vullo V., and Vivio F. 2008. Elastic stress analysis of non-linear variable thickness rotating disks subjected to thermal load and having variable density along the radius, International Journal of Solids and Structures, 45, pp. 5337–5355.

[21] Bayat M., Saleem M., Sahari B., Hamouda A., and Mahdi E. 2008. Analysis of functionally graded rotating disks with variable thickness, Mechanics Research Communications, 35, pp. 283-309.

[22] Zenkour A. M., and Mashat D. S. 2011. Stress function of a rotating variable-thickness annular disk using exact and numerical methods, Engineering, 3, pp. 422-430.

[23] Tütüncü N., and Temel B. 2011. An efficient unified method for thermoelastic analysis of functionally graded rotating disks of variable thickness, Mechanics of Advanced Materials and Structures, 20 (1), pp. 38-46.

[24] Hassani, A., Hojjati, M. H., Farrahi, G. and Alashti, R. A. 2011. Semi-exact elastic solutions for thermomechanical analysis of functionally graded rotating disks, Composite Structures, 93, pp. 3239-3251.

[25] Bayat M., Sahari B. B., Saleem M., Dezvareh E., and Mohazzab A. H. 2011. Analysis of functionally graded rotating disks with parabolic concave thickness applying an exponential function and the Mori-Tanaka scheme**,** IOP Conf. Series: Materials Science and Engineering, 17 012005.

[26] Bayat M., Sahari B. B., and Saleem M. 2012. The effect of ceramic in combination of two sigmoid functionally graded rotating disks with variable thickness, International Journal of Computational Methods, 9 (2), 1240029 (22 pages).

[27] Ghorbani M. T. 2012. A semi-analytical solution for time-variant thermoelastic creep analysis of functionally graded rotating disks with variable thickness and properties, International Journal of Advanced Design and Manufacturing Technology, 5, pp. 41-50.

[28] Amin H., Saber E., and Khourshid A. M. 2015. Performance of functionally graded rotating disk with variable thickness, International Journal of Engineering Research & Technology, 4 (3), pp. 556- 564.

[29] Yıldırım V. 2016. Analytic solutions to power-law graded hyperbolic rotating discs subjected to different boundary conditions, International Journal of Engineering & Applied Sciences (IJEAS), 8 (1), pp. 38-52.

[30] Zheng Y., Bahaloo H., Mousanezhad D., Mahdi E., Vaziri A., and Nayeb-Hashemi H. 2016. Stress analysis in functionally graded rotating disks with non-uniform thickness and variable angular velocity, Int J Mech Sci, 119, pp. 283–293.

[31] Gang M. 2017. Stress analysis of variable thickness rotating FG disc, International Journal of Pure and Applied Physics, 13 (1), pp. 158-161.

[32] Yıldırım V. 2017. Effects of inhomogeneity and thickness parameters on the elastic response of a pressurized hyperbolic annulus/disc made of functionally graded material, International Journal of Engineering & Applied Sciences, 9 (3), pp. 36-50.

[33] Yıldırım V. 2018. A parametric study on the centrifugal force-induced stress and displacements in power-law graded hyperbolic discs, Latin American Journal of Solids and Structures, LAJSS, 15 (4), pp. 1-16.

[34] Young W. C., and Budynas R. G. 2002. Roark's Formulas for Stress and Strain, McGraw-Hill, Seventh Edition, New York.

[35] İnan, M., 1968. The Method of Initial Values and the Carry-Over Matrix in Elastomechanics. ODTU Publication, Ankara, No: 20.

[36] Haktanır V., and Kiral E. 1993. Statical analysis of elastically and continuously supported helicoidal structures by the transfer and stiffness matrix methods, Computers and Structures, 49 (4), pp. 663-677.

[37] Yıldırım V. 1999. In-plane free vibration of symmetric cross-ply laminated circular bars, Journal of Engineering Mechanics-ASCE, 125, pp. 630-636.

[38] Aktas Z. 1972. Numerical Solutions of Two-Point Boundary Value Problems. Ankara, Turkey, METU, Dept of Computer Eng.

[39] Roberts S., and Shipman J. 1979. Fundamental matrix and two-point boundary-value problems, Journal of Optimization Theory and Applications, 28 (1), pp. 77-88.

[40] Haktanır V. 1995. The complementary functions method for the element stiffness matrix of arbitrary spatial bars of helicoidal axes, International Journal for Numerical Methods in Engineering, 38 (6), pp. 1031–1056.

[41] Yıldırım V. 2018. The complementary functions method (CFM) solution to the elastic analysis of polar orthotropic rotating discs, Journal of Applied and Computational Mechanics (JACM) (in press).

[42] Yıldırım V., 2018. Numerical/analytical solutions to the elastic response of arbitrarily functionally graded polar orthotropic rotating discs, Journal of the Brazilian Society of Mechanical Sciences and Engineering (accepted for publication).

[43] Chung Y. L., and Chi S. H. 2001. The residual stress of functionally graded materials, Journal of the Chinese Institute of Civil and Hydraulic Engineering, 3, pp. 1–9.